Test of integral composite panel in compression

NFFP-5, POSCOS

ROLF JARLÅS, JOAKIM SCHÖN, PER DAVIDSSON

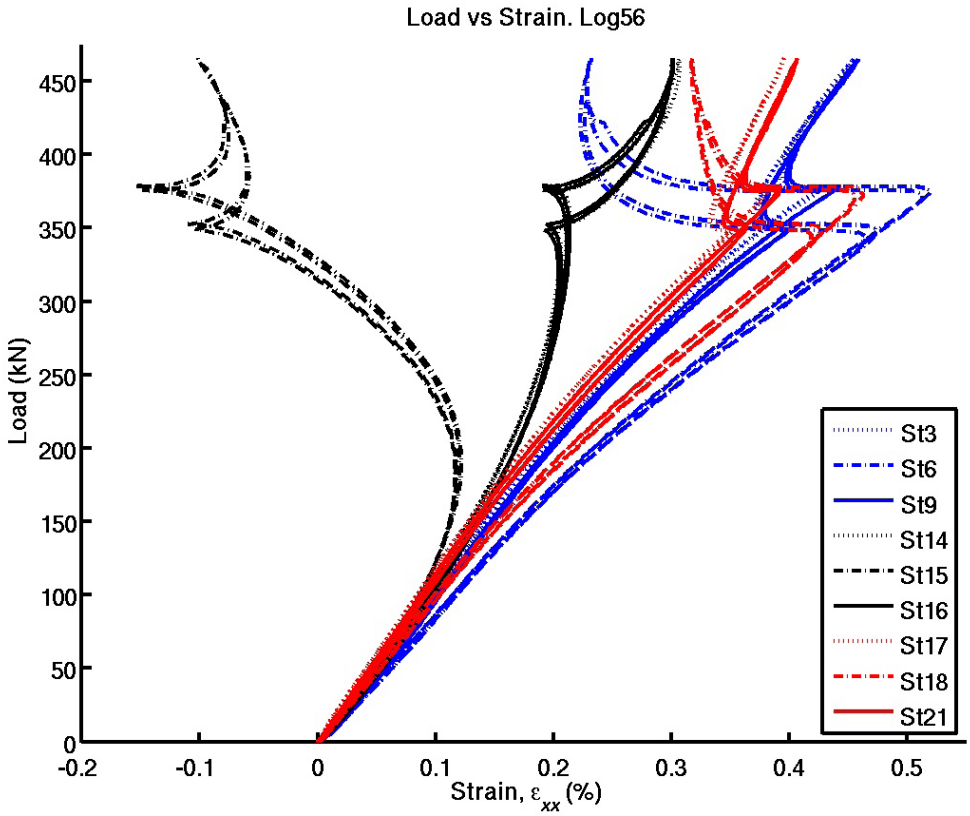

FOI-R--3844-SE
ISSN 1650-1942 January 2014

Rolf Jarlås, Joakim Schön, Per Davidsson

Test of integral composite panel in compression

NFFP-5, POSCOS

Bild/Cover: Strain-gauges indicating nonlinear panel behaviour during compressive load cycles.

Titel	Prov av integralförstyvad kompositpanel i tryck
Title	Test of integral composite panel in compression
Rapportnr/Report no	FOI-R—3844-SE
Månad/Month	Jan
Utgivningsår/Year	2014
Antal sidor/Pages	48 p
ISSN	1650-1942
Kund/Customer	SAAB (NFFP-5 Vinnova)
Forskningsområde	3. Flygteknik och luftstridssimulering
FoT-område	Flygteknik
Projektnr/Project no	E28216
Godkänd av/Approved by	Lars Höstbeck
Ansvarig avdelning	Informations- och aerosystem

Detta verk är skyddat enligt lagen (1960:729) om upphovsrätt till litterära och konstnärliga verk. All form av kopiering, översättning eller bearbetning utan medgivande är förbjuden.

This work is protected under the Act on Copyright in Literary and Artistic Works (SFS 1960:729). Any form of reproduction, translation or modification without permission is prohibited.

Sammanfattning

Projektet POSCOS inom det nationella flygforskningsprogrammet (NFFP) syftar till metodutveckling gällande dimensionering av bucklingsbenägna kompositstrukturer.

I denna rapport rapporteras resultatet av provning gällande en integral förstyvad svagt enkelkrökt komposit-panel som belastats i tryck (POSCOS-2). Panelen tillverkades av SAAB AB och provningen genomfördes vid FOI. Provresultaten som beskrivs här innefattar last-, töjnings- och fullfälts-mätningar med det optiska systemet Aramis. Provningen visar att kollapslasten är cirka 2,5 gånger högre än bucklingslasten för skinnet, samt att ett mindre antal lastcykler till nivåer avsevärt högre än bucklingslasten kan göras utan att medföra några observerbara skador eller mätbara resttöjningar.

Provresultaten som beskrivs i denna rapport kan jämföras med motsvarande prov för en byggd panel med förstyvningar i aluminium som skruvats fast mot en plan komposit-platta (POSCOS-1).

Nyckelord:

komposit, panel, integral panel, buckling, prov, test, tryck

Summary

The project POSCOS within the Swedish National Aeronautical Research program (NFFP) aims at methods development regarding strength prediction and sizing-methods for buckling-critical composite structures. The test results are reported for an integrally stiffened slightly curved composite panel loaded in compression (POSCOS-2). The panel was produced by SAAB AB, and the testing was performed at FOI. The test-results contain load-, strain- and full-field measurements using the optical system Aramis. The measurements show that the collapse load is approximately 2.5 times higher than the buckling load for the skin. It is also found that applying a limited number of load-cycles well above the buckling load do not cause any observable damage or measurable residual strain.

The results presented can be compared with those for a similar test performed on a panel where aluminium-stringers were bolted to a flat composite skin (POSCOS-1).

Keywords: composite, panel, integral panel, buckling, test, compression

Contents

1 Introduction

Composites are often used to reduce weight in aircraft structures. Some structures, or part of structures, will be subjected to compressive loading and as a result buckling might occur. For such cases the buckling load is often the factor that drives the design. Buckling in composite structures is currently not allowed at operational loads. Allowing it would enable a considerable reduction in weight. Considerable work has been done in the past on buckling of monolithic structures made of aluminium. There are handbooks on how to estimate the buckling load and numerical methods have been verified. A large number of experiments have been done in the past. Composites are orthotropic and equations for monolithic materials are not necessarily valid. Therefore, numerical methods and handbook methods need to be developed for composites. That has been done in another part of the project. Those methods need to be validated against experiments and this report describes such an experiment.

The objective of the investigation has been to determine buckling displacement shape for an integral composite panel. Strain gauges are attached at several points to measure strain and strain redistribution due to nonlinear effects, with high accuracy and to determine the load required to cause subsequent residual strain caused by dissipation and damage. To determine the compressive failure load of the specimen is also included as an objective. The panel was produced by SAAB AB, and the testing was performed at FOI.

2 Experimental Procedure

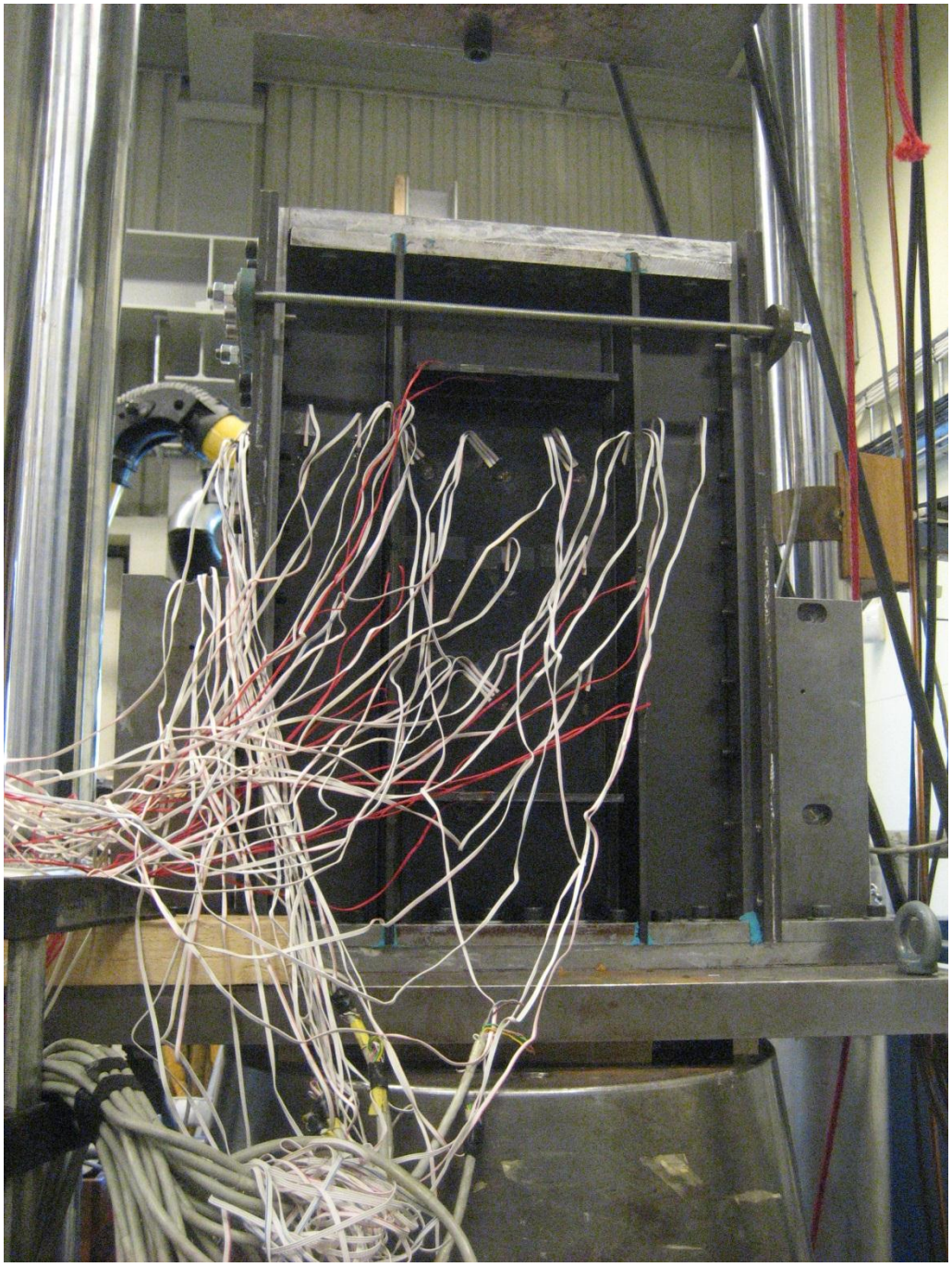

Figure 2.1 Specimen with strain gauges mounted in the test rig

2.1 Test rig and boundary conditions

The specimen was mounted in a test rig, see Fig. 2.1. The lower and upper edge of the specimen was placed on wide thick flat steel plates. Around the lower and upper sides of the specimen edges there were smaller 20 mm thick steel plates, mounted with bolts to the wide flat plates. The tracks formed between the smaller steel plates were about 8-10 mm

wider than the thickness of skin and stiffener. These tracks were completely filled with epoxy to obtain clamped conditions at the lower and upper edges of the panel. The upper steel plate was guided by the rig and movable vertically, following the stroke in a load frame. The two straight vertical edges of the panel were mounted without applying pressure between straight adjustable steel rulers with sharp edges to obtain simple support conditions.

To apply the compressive loading on the specimen the rig was placed on top of the lower grip in a MTS hydraulic testing machine with a capacity of 1000 kN. The lower grip was moved upward until contact was made with the upper grip and compression could be applied, see Fig. 2.2. The applied force and grip displacement were measured with the sensors in the load frame. In addition a laser extensiometer, optoNCDT 1300 from micro-epsilon with 100 mm measurement range, was placed on the right side of the rig and was attached with a ferrule, see Fig. 2.2. The extensiometer measured the distance to the thick steel plate on the upper grip.

Figure 2.2 Specimen mounted in the test rig and load frame

2.2 Panel geometry

The panel is illustrated in Fig. 2.3. The panel has a cylindrical skin with a radius of 4084 mm[1], width 400 mm and height 580 mm. Nominal skin thickness is 3.12 mm. There are two long vertical stringers, co-cured and designed as blades without a stringer-foot. The stringer-height is 60 mm and measured blade-thickness was 6.5 mm. The distance (arc-length) between the blades is 200 mm.

There are short (170 mm) horizontal integral rib-foots between the stringers close to the upper and lower horizontal edges of the panel. These rib-foots are T-shaped, symmetric and with tapered flanges. The free web is 60 mm high and 6.5 mm thick, with a horizontal plane of symmetry located 115 mm from the upper or lower edge of the panel. The thickness of the flanges ranges from 3.3 mm to zero.

A straight ruler was used to find any waviness in the skin. The panel was found to be everywhere straight in the x-direction to within 0.2 mm on the stringer-free side of the skin.

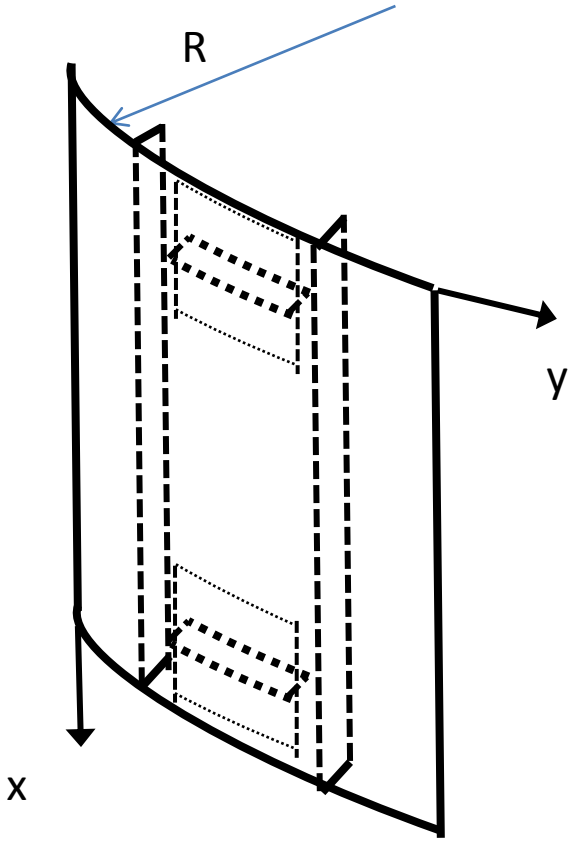

Figure 2.3 Panel design principle

[1] Determined by measuring the sagitta (gap to a flat surface(Swedish:pilhöjd)), being 4.9 mm

2.3 Panel material properties and layup

The composite skin is almost quasi-isotropic, but with reduced number of plies in the $\pm 45^{o}$-directions, whereas the vertical stringers have more fibres in the loading-direction than in the horizontal direction. The composite properties for the panel are summarized in Table 2.1, with reference to SAAB for more detailed questions.

Table 2.1 Composite properties

	Skin	**Stringer**
% 0	33.3	41.7
% ±45	33.4	41.6
% 90	33.3	16.7
E_{11} (MPa)	60783	71526
E_{22} (MPa)	60783	42013
G_{12} (MPa)	15233	17699
G_{13} (MPa)	5190	5190
ν_{12}	0.2052	0.3432

2.4 Load sequence

During loading of the specimen the displacement of the grip was controlled. The load sequence is schematically illustrated in Fig. 2.4. The coordinate system was adjusted such that zero was when the rig made contact with the upper grip. Before testing begun the lower grip was moved such that it was 0.2 mm below zero, the rig was not in contact with the upper grip. The specimen was then loaded at 1 mm/min rate until the first prescribed maximum stroke was reached where it was hold for 15 s. It was then unloaded at 1 mm/min until the stroke reached -0.2 mm and the specimen rig was not in contact with the upper grip. The procedure was then repeated one more time with a larger maximum stroke. The maximum stroke was then increased for the next set of two cycles. During the two displacement cycles all signals measured were recorded and stored. Data from the measurements were gathered in blocks, called Logs, where each Log typically contains data for two load-cycles. The relation between Log number, cycle number, maximum stroke and maximum load is presented in Table 2.2.

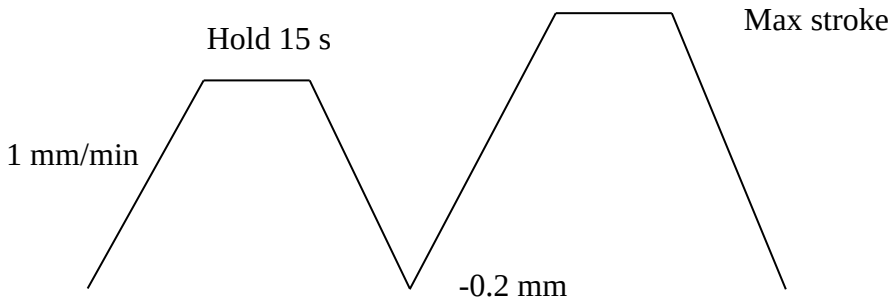

Figure 2.4 Schematic of displacement controlled test cycle

Table 2.2 Data from displacement cycles.

Log No.	Cycle	max Stroke (mm)	max Load (kN)	Remark
46	1	0.4	7	
	2	0.8	44	
48	1	1.2	101	
	2	1.6	161	
50	1	2.0	220	
	2	2.4	285	
52	1	2.8	345	
	2	3.0	372	
54	1	3.2	393	Sound related to displacement mode switch
	2	3.4	418	
56	1	3.6	437	
	2	3.8	466	
58	1	4.0	488	
	2	4.2	509	Visible stiffener buckling
60	1	4.4(almost)	524	Damage
62	1		414	Weakened

2.5 Strain gauge measurements

A total of 62 strain-gauges, 350 ohm and 5 mm gauge length, were used, located as illustrated in Fig. 2.5. Their coordinates are given by Table 2.3. The origin is at the corner of the specimen as schematically shown in Fig. 2.5. Gauges are attached on both sides of the composite skin and on the stringers to make it possible to determine membrane- and bending strains, to monitor load redistribution due to buckling, and to determine when buckling occurs. The gauges measuring strain in the direction of the applied load (X) are located at three different X-coordinates (190, 290 and 390 mm) from the top of the panel. This means that the second row of gauges was on the line of symmetry for the panel. There were three columns with gauges between the stringers. With nominal values these are at Y=133, 200 and 266 mm, and two columns outside of each stringer at Y=30, 75, 325 and 370 mm. To get an indication of bending of the stringer blade and lifting from the skin there were 12 gauges measuring strain in the radial direction (Z) on the stringers.

Table 2.3 strain gauge positions

(Measured positions, for plate measured to be 402 mm wide.
F=smooth side, B=stiffener side, S=stiffener or stringer, D=direction measured,
z=distance to skin on stiffener side)

No.	Skin smooth side
1	Fx=190, y=30.0, D=x
2	Fx=190, y=75, D=x
3	Fx=190, y=134, D=x
4	Fx=190, y=134, D=y
5	Fx=190, y=134, D=-x,y
6	Fx=190, y=201, D=x
7	Fx=190, y=201, D=y
8	Fx=190, y=201, D=-x,y
9	Fx=190, y=268, D=x
10	Fx=190, y=268, D=y
11	Fx=190, y=268, D=-x,y
12	Fx=190, y=332.7, D=x
13	Fx=190, y=372, D=x
14	Fx=290, y=134, D=x
15	Fx=290, y=201, D=x
16	Fx=290, y=268, D=x
17	Fx=390, y=134, D=x
18	Fx=390, y=201, D=x
19	Fx=390, y=201, D=y
20	Fx=390, y=201, D=-x,y
21	Fx=390, y=268, D=x

No.	Skin stiffener side
22	Bx=190, y=30, D=x
23	Bx=190, y=75, D=x
24	Bx=190, y=134, D=x
25	Bx=190, y=134, D=y
26	Bx=190, y=134, D=-x,y
27	Bx=190, y=201, D=x
28	Bx=190, y=201, D=y
29	Bx=190, y=201, D=-x,y
30	Bx=190, y=268, D=x
31	Bx=190, y=268, D=y
32	Bx=190, y=268, D=-x,y
33	Bx=190, y=327, D=x
34	Bx=190, y=372, D=x
35	Bx=290, y=134, D=x
36	Bx=290, y=201, D=x
37	Bx=290, y=268, D=x
38	Bx=390, y=134, D=x
39	Bx=390, y=201, D=x
40	Bx=390, y=201, D=y
41	Bx=390, y=201, D=-x,y
42	Bx=390, y=268, D=x

No.	Upper short stiffener
43	Sx=75.5, y=201, z=45, D=y
44	Sx=80, y=201, z=45, D=y
No.	Long vertical stringers
45	Sx=190, y= 96, z=15, D=z
46	Sx=190, y= 96, z=15, D=x
47	Sx=190, y=102.5, z=15, D=z
48	Sx=190, y=102.5, z=15, D=x
49	Sx=190, y=303.5, z=15, D=z
50	Sx=190, y=303.5, z=15, D=x
51	Sx=190, y=310, z=15, D=z
52	Sx=190, y=310, z=15, D=x
53	Sx=290, y= 96, z=15, D=z
54	Sx=290, y=102.5, z=15, D=z
55	Sx=290, y=303.5, z=15, D=z
56	Sx=290, y=310, z=15, D=z
57	Sx=390, y= 96, z=15, D=z
58	Sx=390, y=102.5, z=15, D=z
59	Sx=390, y=303.5, z=15, D=z
60	Sx=390, y=310, z=15, D=z
No.	Lower short stiffener
61	Sx=500, y=201, z=45, D=y
62	Sx=504.5, y=201, z=45, D=y

The strain gauges were excited with 2 V or 5 V and the change in resistance was measured with FFA bridge amplifiers. The strain gauges were connected to a Wheatstone bridge with two wires. The amplifiers used a fixed gain of 50 or 100 times. The strain was calculated directly in the data acquisition system based on the gauge factor and amplifier gain. In addition shunt calibration with 10 kOhm resistance was done but not used when calculating strain.

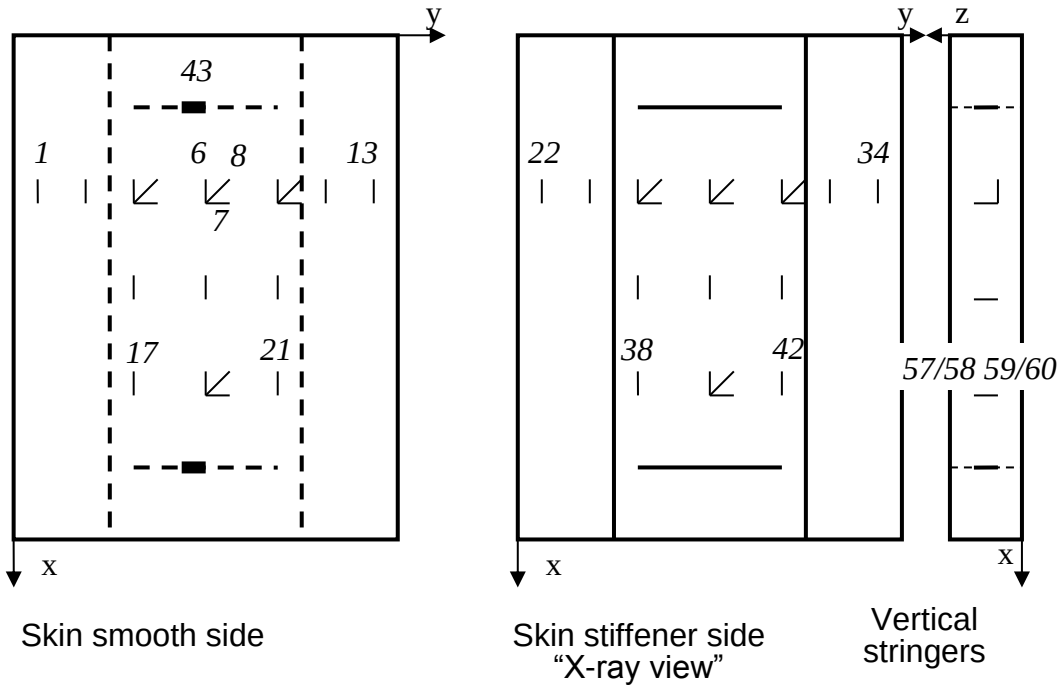

Figure 2.5 Illustration of strain-gauge positions and orientation. Numbering from left to right, top to bottom, smooth side then stiffener side. (Orientation of rosette diagonal may be 90°-different from illustration)

2.6 C-scan

After failure two areas of the specimen was C-scanned to see if there are any delaminations. The specimen was submerged in water and a 10 MHz transducer was swept over the surface. An A-scan was also used to look for delaminations after failure.

2.7 Speckle photography, (Aramis)

The skin smooth side of the specimen was spray painted black and then a white colour was sputtered onto the surface to create a speckle pattern (a random irregular pattern of dots). A picture of the surface can be seen in Fig. 2.6. Two cameras were placed about 625 mm from the surface a distance 308 mm apart, see Fig. 2.2. The camera angle is 25°. This gives a measurements area of approximately 500x420 mm^2. Depth of focus was large due to a large aperture for the lenses. Pictures of the specimen were taken before loading and then every fifth or tenth seconds until the load cycle was finished. Since the maximum compressive load was kept constant for 15 s, a picture was always taken at the maximum load. The pictures were analysed with Aramis commercial software. The origin in the Aramis system is approximately at the central strain gauge, x=290 mm and y=201 mm in the specimen coordinate system.

A pair of photos taken by the cameras, as reference for Log 56 is shown in Figs. 2.7-8. A green region marks where Aramis will be able to evaluate displacements, if the same spot is also green on the picture from the other camera.

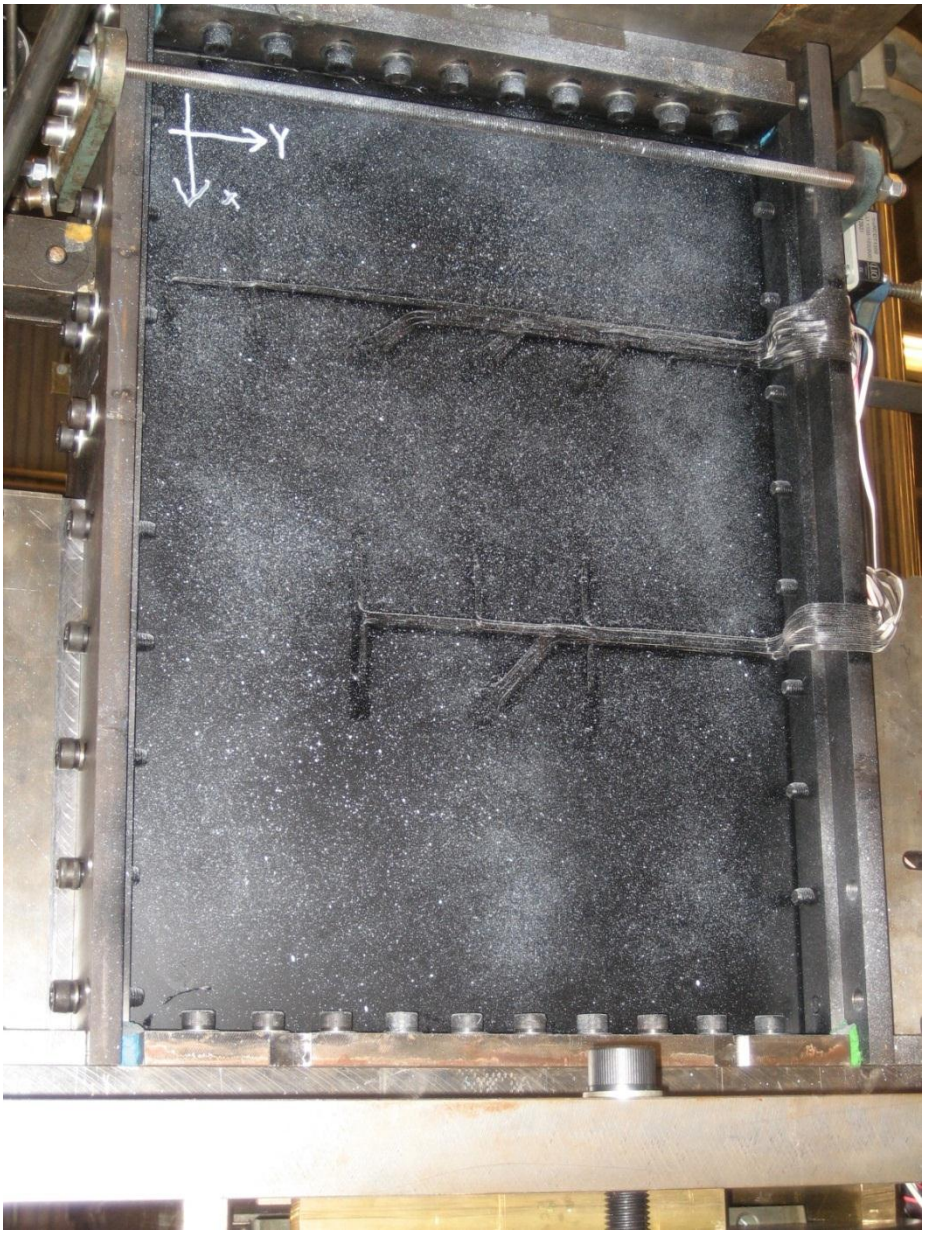

Figure 2.6 Specimen smooth side with speckle “dots” for Aramis

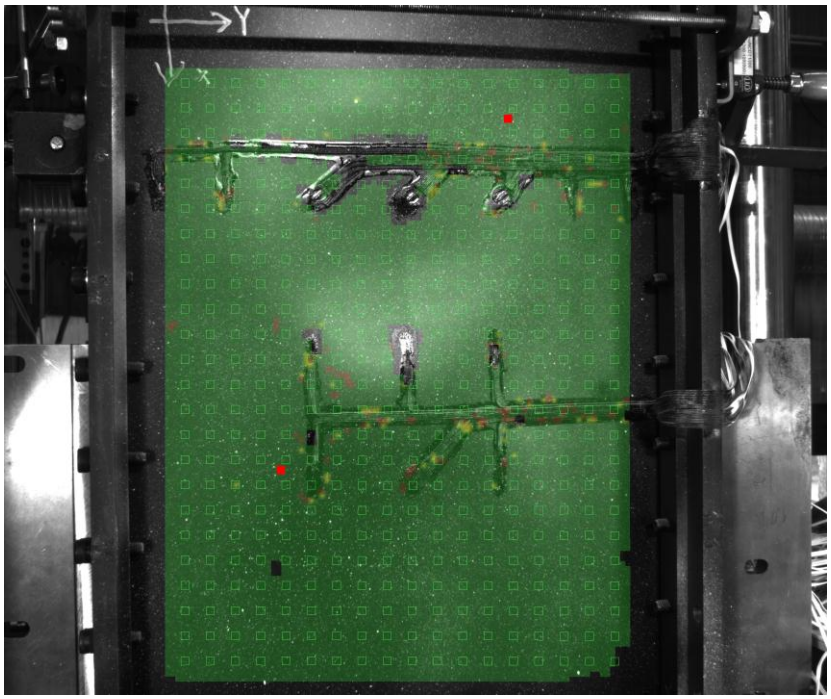

Figure 2.7 Photo taken by the left camera as reference for Log 56. The green region marks where Aramis will be able to evaluate displacements, when the region is also green on the corresponding picture from the right camera

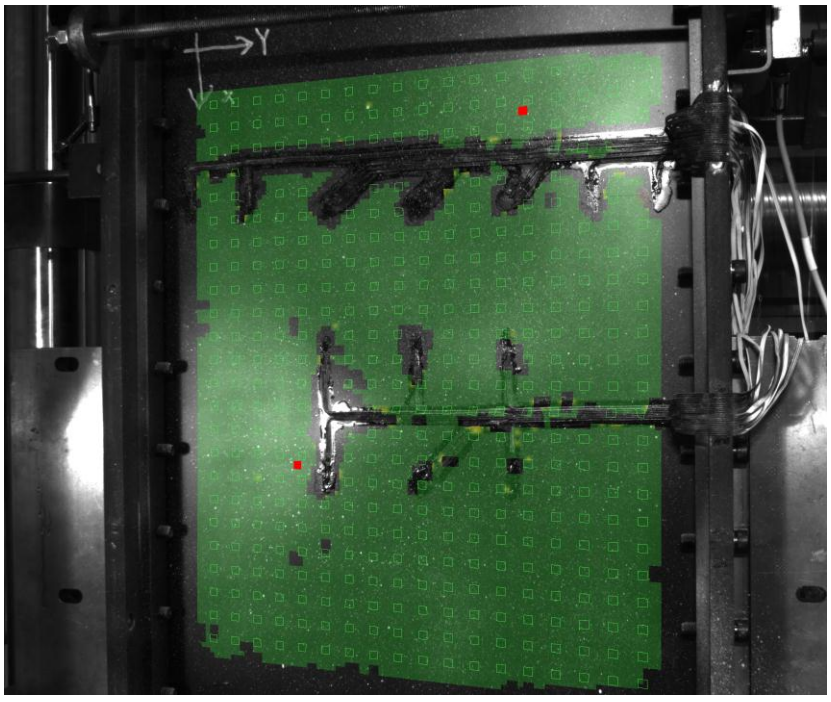

Figure 2.8 Photo taken by the right camera as reference for Log 56

3 Results

During loading a compressive force was applied to the specimen. To show compressive forces, compressive strains and compressive grip displacement as positive the measured values have been scaled by -1 before being shown in figures.

3.1 Stroke response during load cycles

The grip displacement measured with the transducer in the load frame, and the displacement measured with the laser extensiometer placed on the test rig, are both shown in Fig. 3.1. The displacement from the load frame is used by the controller and therefore it behaves fairly well. At maximum displacement the displacement is kept constant for 15 s which can be seen in Fig. 3.1. The displacement measured with the laser extensiometer behaves similar to the grip displacement. The signal shows large oscillations which might be due to friction between the specimen and the rig holding the specimen and the laser extensiometer. During the second load cycle the maximum displacement from the laser extensiometer is less than during the first load cycle. Since the force is larger for the second load cycle than the first load cycle the laser extensiometer signal is obviously not correct. For better measurements the extensiometer should be connected directly to the plate loading the specimen. The grip displacement is probably larger due to elastic deformation than the actual displacement of the specimen. Most results will for this reason be presented as a function of the applied load, as measured by the load cell in the testing machine.

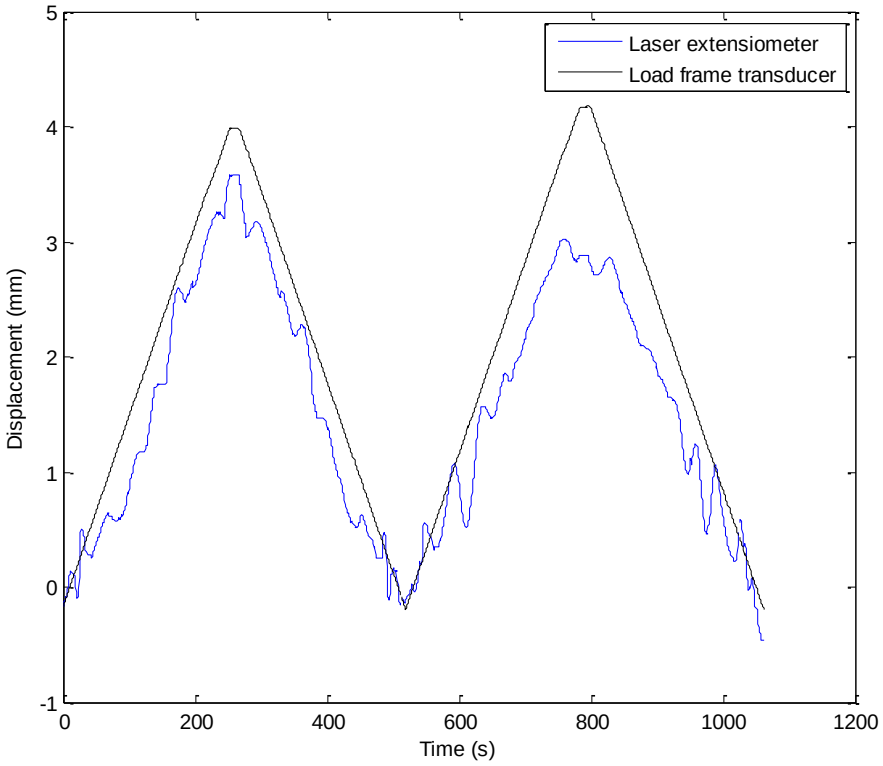

Figure 3.1 Displacement measurements for Log 58

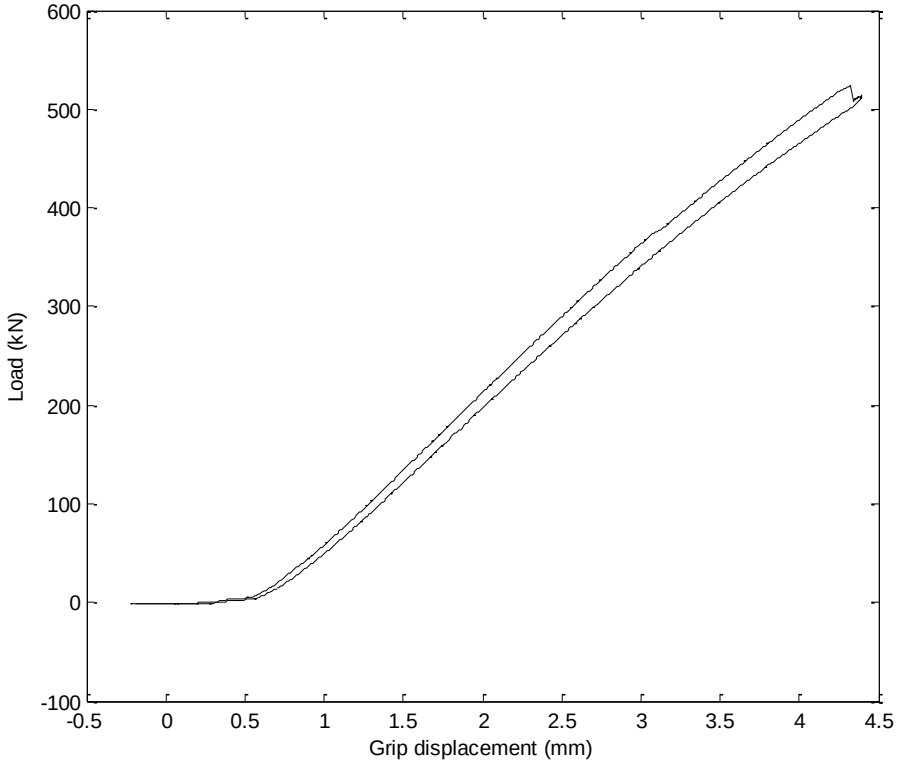

Figure 3.2a Load as a function of grip displacement for the last load cycle, Log 60

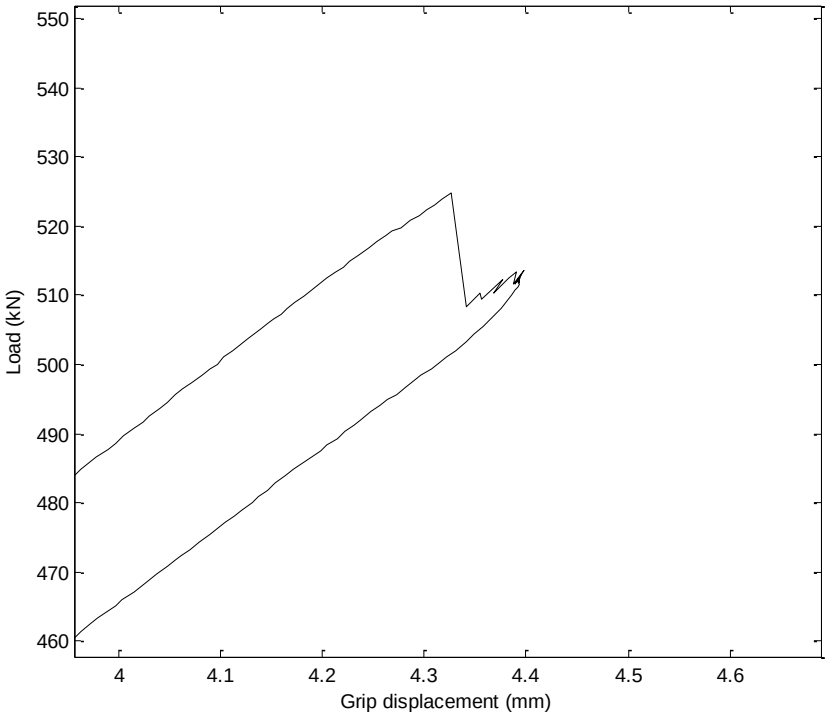

Figure 3.2b Load as a function of grip displacement for the part of the last load cycle, (Log 60), when the specimen breaks

The load versus grip displacement shown in Fig. 3.2a is for the load cycle when the specimen breaks. After failure the specimen nearly returns to its original grip displacement when the load is removed. The part of the figure showing when failure occurred is magnified in Fig. 3.2b and at failure the load drops about 15 kN and then as the grip displacement increases the load increases.

3.2 Aramis measurements

The out of plane displacement as measured by the Aramis-system is shown at a load of 331 kN in Fig. 3.3. As may be seen the system fails to measure displacements where the vires for the strain-gauges are attached. Displacements towards the cameras are defined as positive by the Aramis system. The result shows a central buckle between the stringers with an amplitude of about 3 mm and pointing towards the cameras. This measurement can be compared with the corresponding measurement in Fig. 3.4 at 395 kN, which shows that there are now two buckles below each other that are pointing to opposite directions.

In Figs. 3.5-3.8 the out of plane displacement at 331 kN are shown for the four passages of this load-level in Log 56. The difference is very small, but it is possible to see that the border between the upper blue and the green region is moved slightly downwards during the unloading (Figs. 3.6&3.8), as compared to the photos taken during loading (Figs. 3.5&3.7). Similarly in Figs. 3.9-3.12 the out of plane displacement at 395 kN are shown. The differences between the four measurements are as may be seen extremely small.

The in-plane vertical displacement at 331 kN and 395 kN measured with Aramis are shown in Figs. 3.13 and 3.14 respectively. The vertical distance between the upper and lower boundary of the region evaluated by Aramis is about 440 mm for this setup. Evaluating the displacement in Fig. 3.13 in the middle of the panel at the upper and lower edge of the Aramis-region, we read 1.4 and 2.55 mm respectively. This gives an average strain of 0.26 % at 331 kN. Similarly at 395 kN the average is approximately 0.45%.

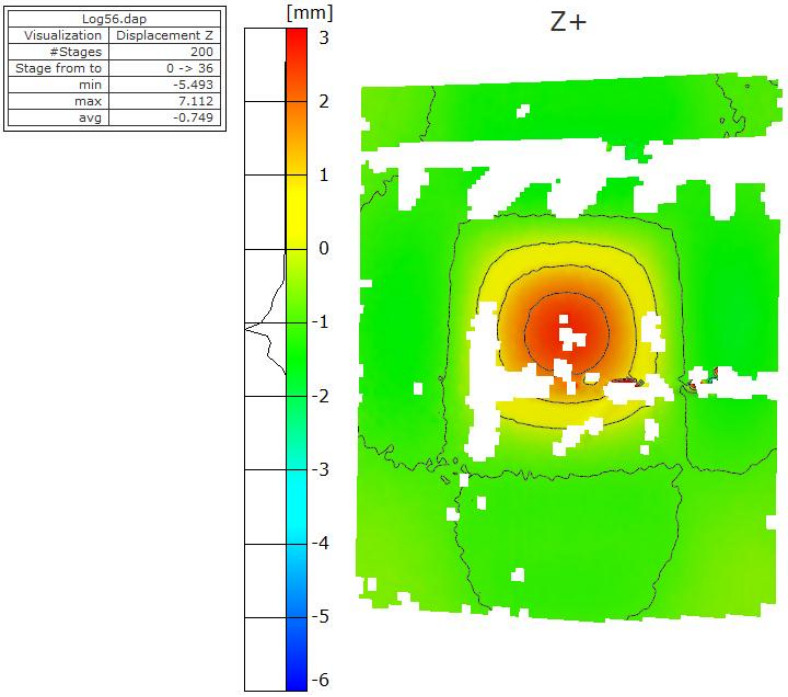

Fig 3.3 Log 56 331 kN cycle 1 180 sec (loading) Out of plane displ. Range[-6,3] mm

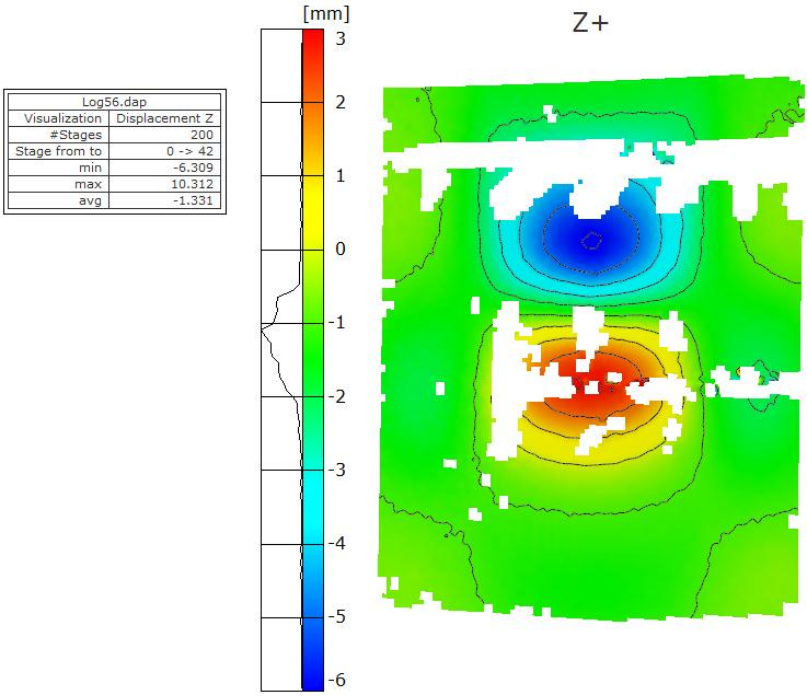

Fig 3.4 Log 56 395 kN cycle 1 210 sec (loading) Out of plane displ. Range[-6,3] mm

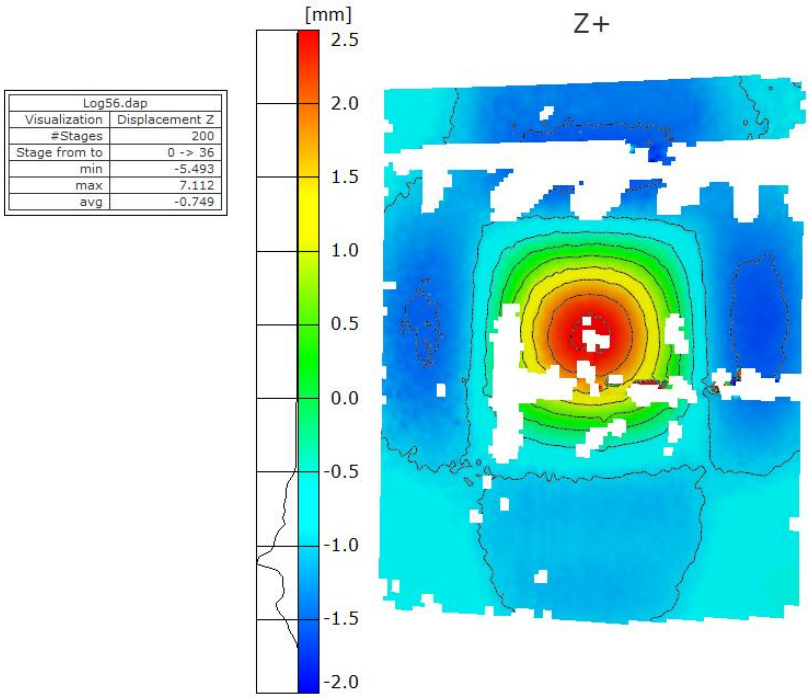

Fig 3.5 Log 56 331 kN cycle 1 180 sec (loading) Out of plane displ. Range[-2,2.5] mm

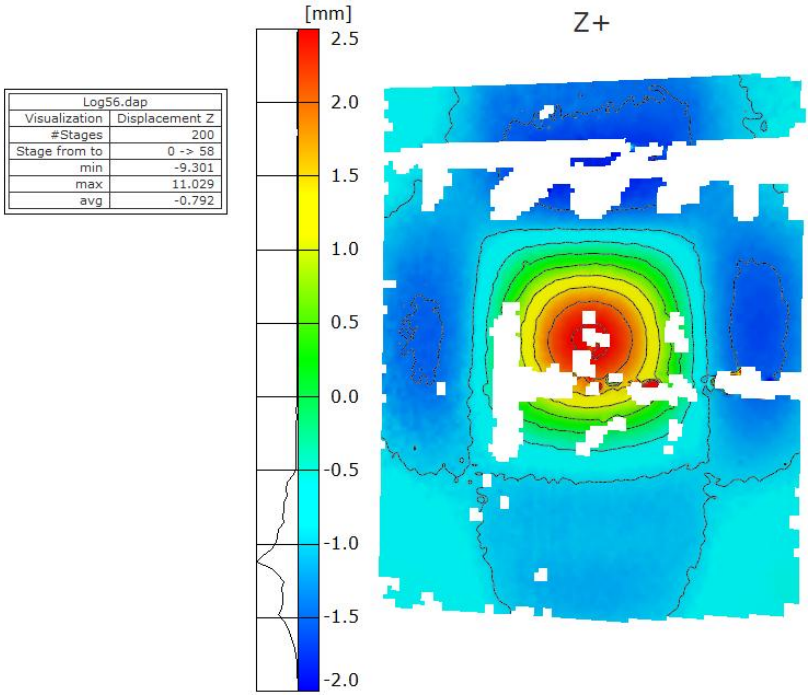

Fig 3.6 Log 56 331 kN cycle 1 290 sec (unload) Out of plane displ. Range[-2,2.5] mm

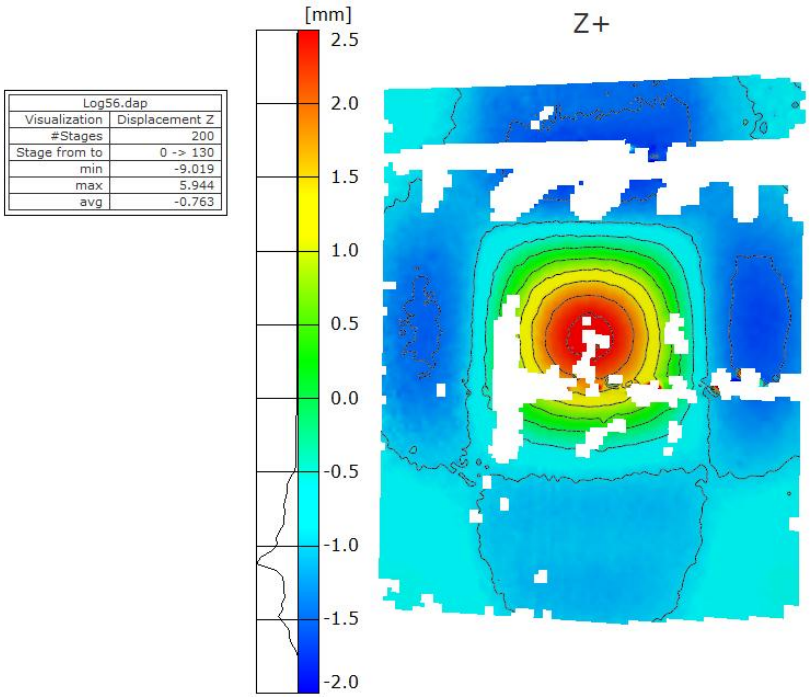

Fig 3.7 Log 56 331 kN cycle 2 650 sec (loading) Out of plane displ. Range[-2,2.5] mm

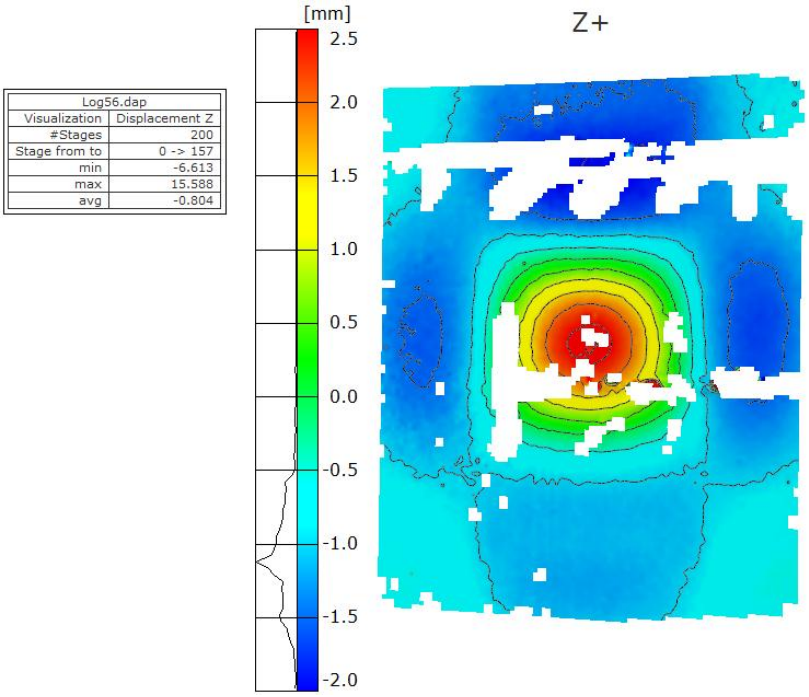

Fig 3.8 Log 56 331 kN cycle 2 785 sec (unload) Out of plane displ. Range[-2,2.5] mm

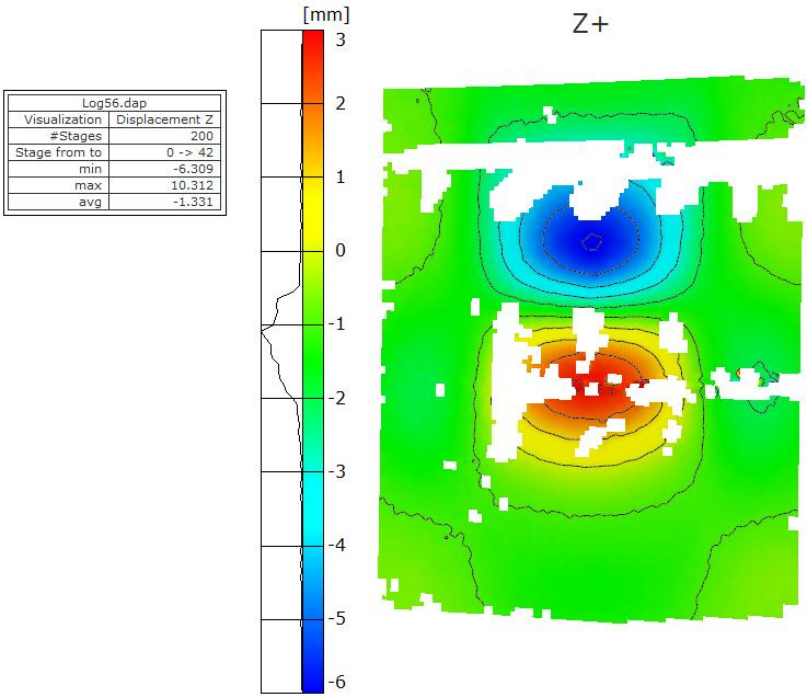

Fig 3.9 Log 56 395 kN cycle 1 210 sec (loading) Out of plane displ. Range[-6,3] mm

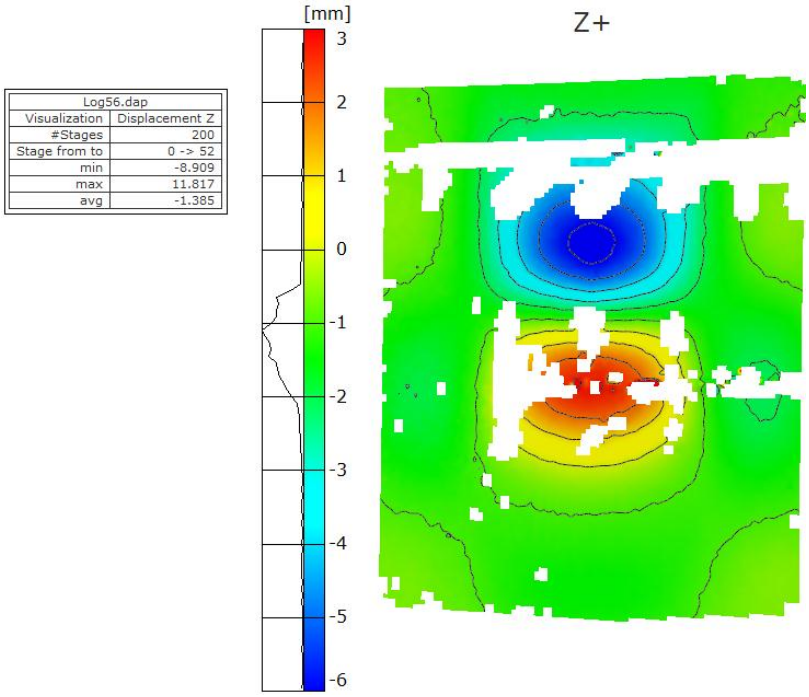

Fig 3.10 Log 56 395 kN cycle 1 260 sec (unload) Out of plane displ. Range[-6,3] mm

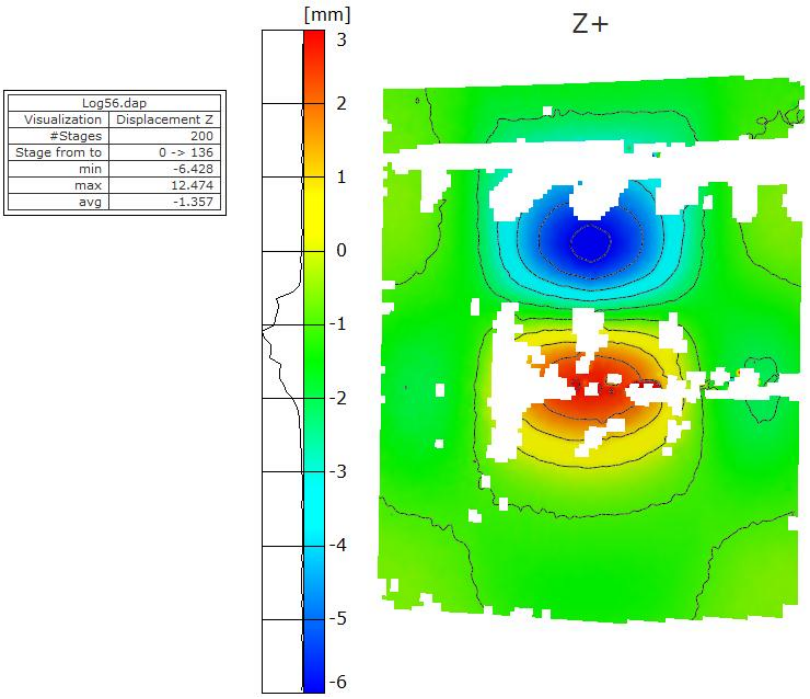

Fig 3.11 Log 56 395 kN cycle 2 680 sec (loading) Out of plane displ. Range[-6,3] mm

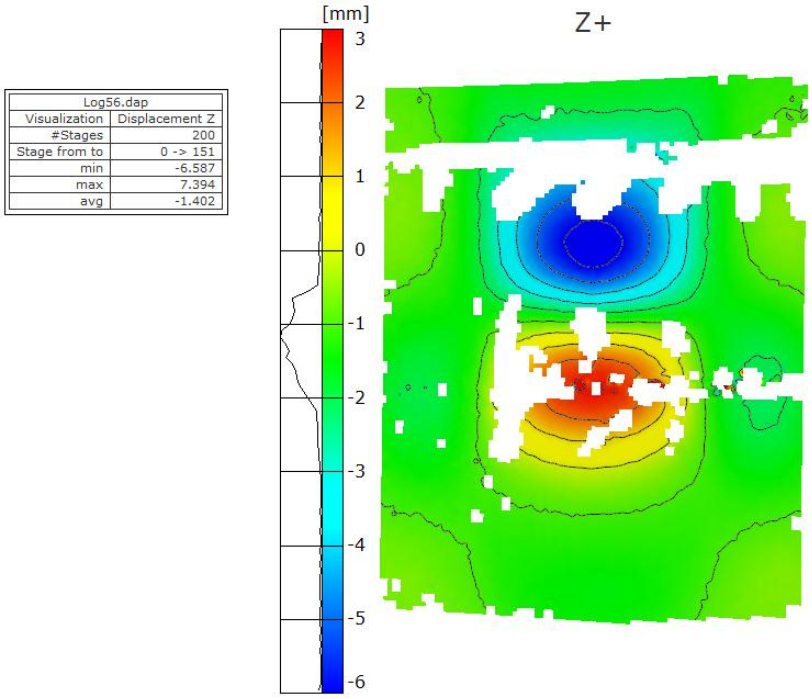

Fig 3.12 Log 56 395 kN cycle 2 755 sec (unloading) Out of plane displ. Range[-6,3] mm

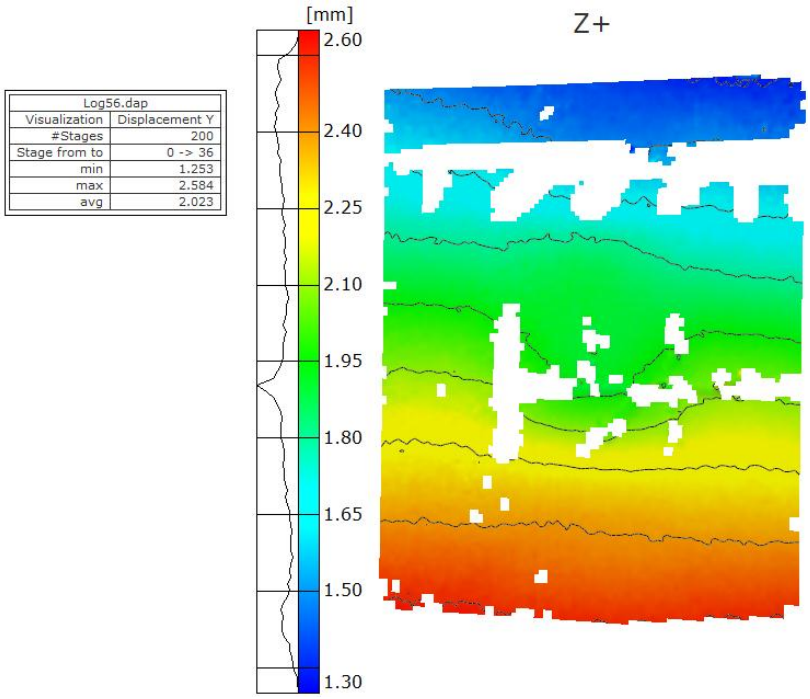

Fig 3.13 Log 56 331 kN cycle 1 180 sec (loading) In plane displ. Range[1.3,2.6] mm

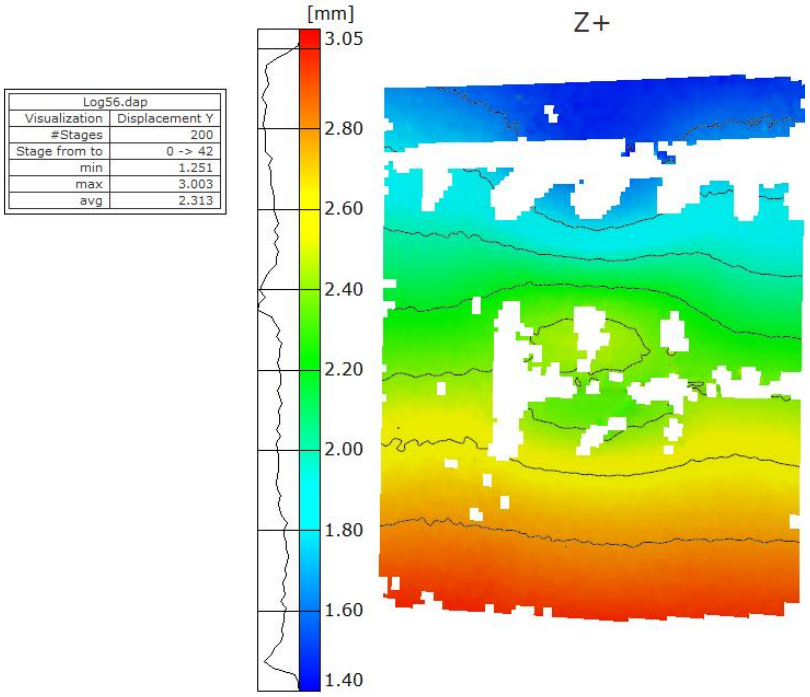

Fig 3.14 Log 56 395 kN cycle 1 210 sec (loading) In plane displ. Range[1.4,3.05] mm

Strain in the vertical direction as evaluated by Aramis at 331 kN is shown in Fig. 3.15. The results contain some scatter as a consequence of the resolution in the speckle dots and the cameras. The strain is fairly constant outside of the stringers, with compressive strain near -0.3%. It is also seen that the strain near the middle of the panel is slightly tensile, but below 0.1%. It is concluded that buckle in the middle of the panel at a load of 331 kN is convex, when seen from the smooth side (the camera side).

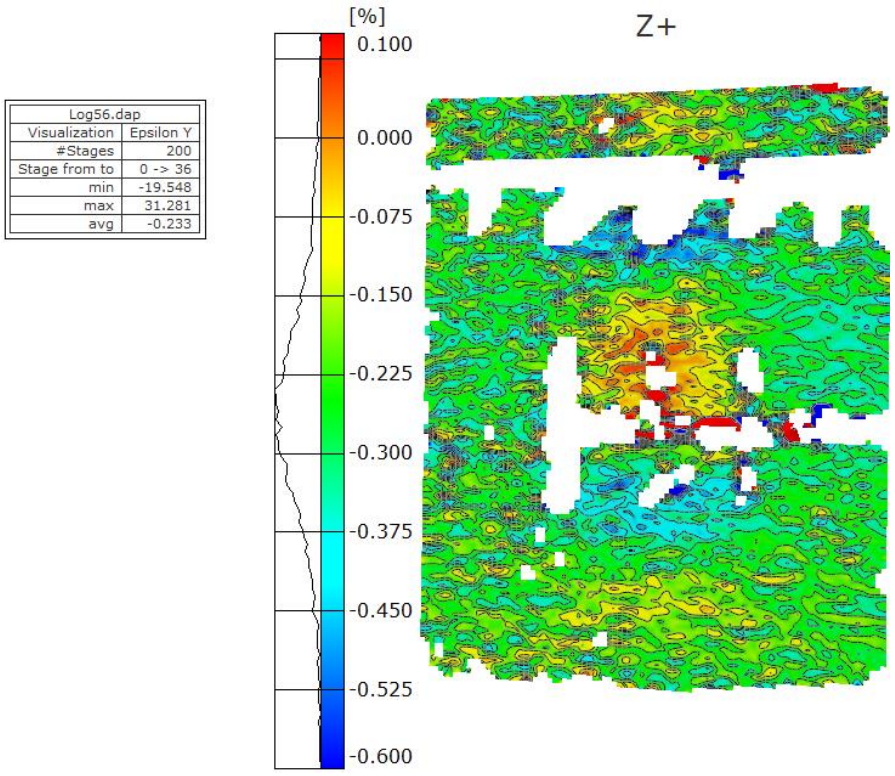

Fig 3.15 Log 56 331 kN cycle 1 180 sec (loading) Strain in load direction (%).

3.3 Strain gauge results

A total of 62 strain-gauges were attached as described in section 2.5. Compressive load and compressive strain will be defined as positive in the discussion and in the graphs below.

At first we look in Fig 3.16 for expected symmetries in strain for gauges on the stringer-free side of the panel, located on each side of the lines of symmetry in the panel. Due to symmetry the measured strain for gauge 14 and 16 as well as for gauge 6 and 18 are expected to coincide. It is seen that gauge 6 is strained faster initially than the other gauges, before showing a linear response above 10 kN. The difference in strain between gauge 6 and 18 is slowly increasing as the load increases, all the way to the maximum load in this load cycle. Measured strain in gauge 14 and 16, are in good agreement but with a slightly higher strain in gauge 16. The results are similar for gauges 35 and 37 on the stiffener side, indicating good symmetry with respect to the vertical plane through Y=200. Strain reversal for gauge 15 at approximately 195 kN is also observed. The strain reversal load is sometimes referred to as the buckling load.

As gauge 36 on the stringer-side is more strained than gauge 15 on the smooth side it is concluded that the stringer side of the panel skin is bending to become concave. The behaviour for gauges 6 and 18 are similar as for gauge 36, indicating that they are also on the concave side of a buckle. As speckle-measurements showed earlier (Figs. 3.5-3.8) there is for the loads shown here a large buckle developing in the centre of the plate, and smaller buckles in the opposite direction above and below the central buckle.

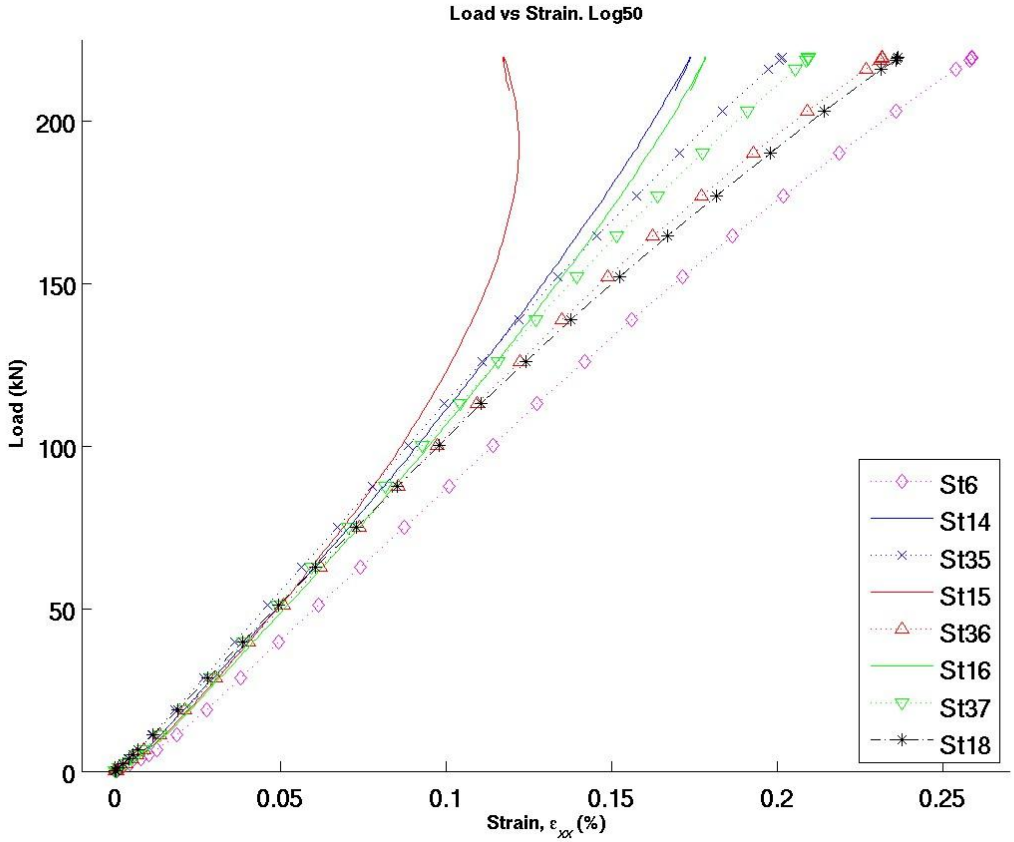

Figure 3.16 Strain in the loading direction for gauges on the skin

The measured strain in the loading direction are shown in Fig. 3.17 during the two cycles in Log52, for the gauges at X=190 on the stringer side.

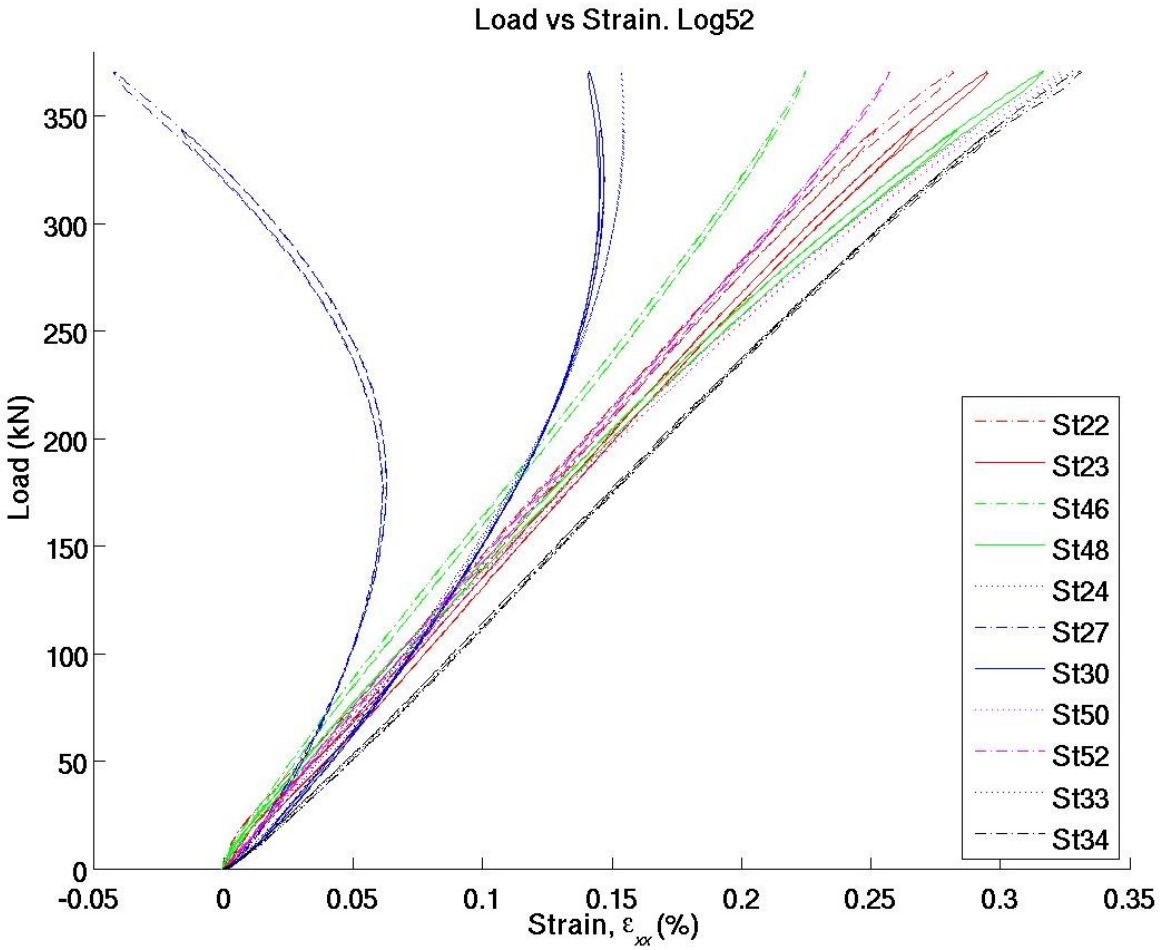

Figure 3.17 Strain in the loading direction for gauges on the stiffener side of the panel

Two load-cycles are shown in Fig. 3.18. Looking at the curve for gauge 15 it may be seen that the loading and unloading paths are slightly different. Each of them is practically identical between cycle one and two below 300 kN, showing no influence from the difference in previous maximum load.

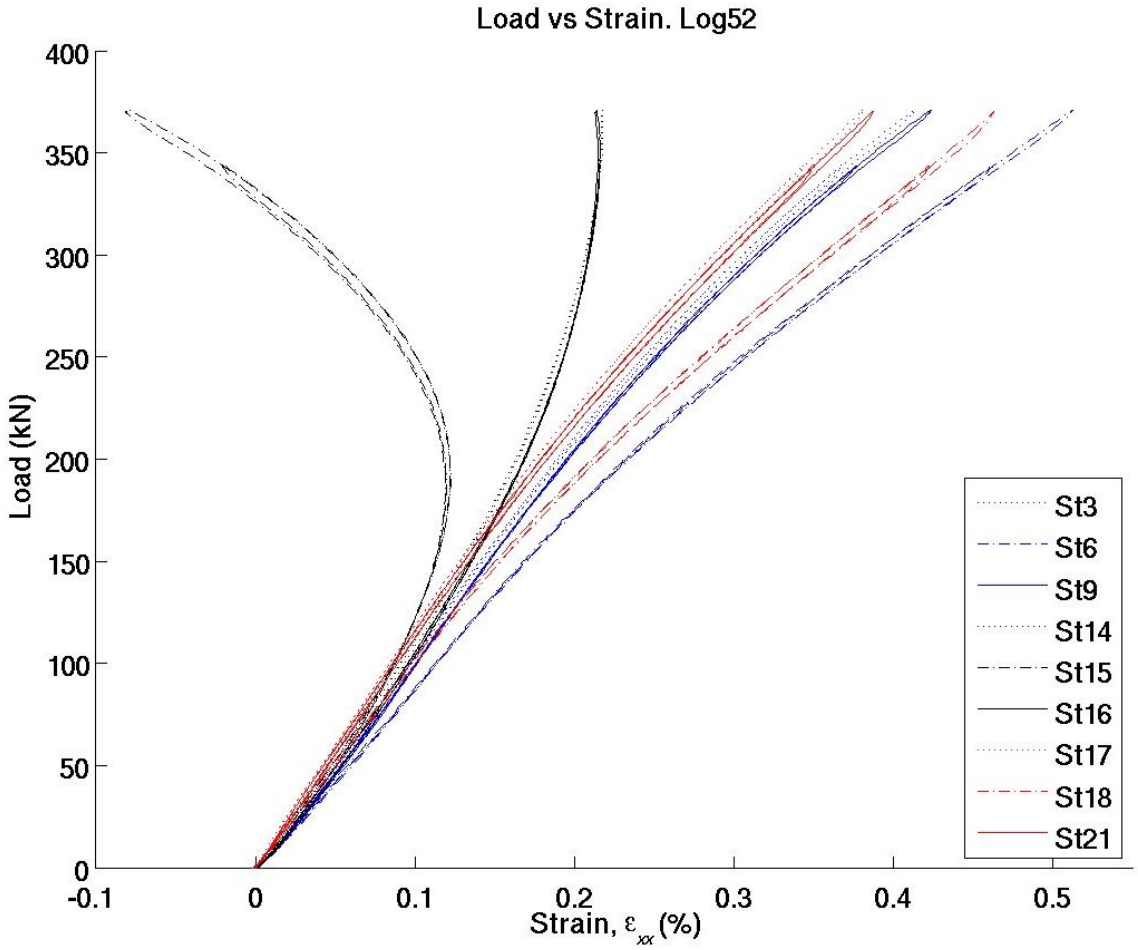

Figure 3.18 Strain for gauges on the smooth side of the skin. Log 52

The non-linearity in strain response reaches a new level near 380 kN as shown in Fig. 3.19. Points **A-E** are reached in that order and was as described above subject to further analysis with the Aramis system. Gauges 6 and 18 don't follow each other above 380 kN indicating that the symmetry in the deformation with respect to the horizontal symmetry plane at X=290 is lost. The curves show two load-cycles to different maximum levels, but following almost the same path during unloading. This indicates that the panel is still intact, and that the distinct sound heard together with the buckling-mode switch at 380 kN during loading is not associated with damage growth. It is interesting to observe that the buckling mode switch at unloading is noiseless and delayed, occurring at 350 kN. Some of the curves are in principle horizontal at 380 kN during loading, which by definition is loss of uniqueness with respect to applied load. The same curves have a small but non-zero slope near 350 kN which is in agreement with the silent springback during unloading. There is also something happening in the first cycle near 415 kN affecting gauges 6 and 16. While gauge 6 becomes slightly less strained gauge 16 becomes more strained. This is not repeated in the second cycle, almost closing the gap between the two pair of curves above 415 kN.

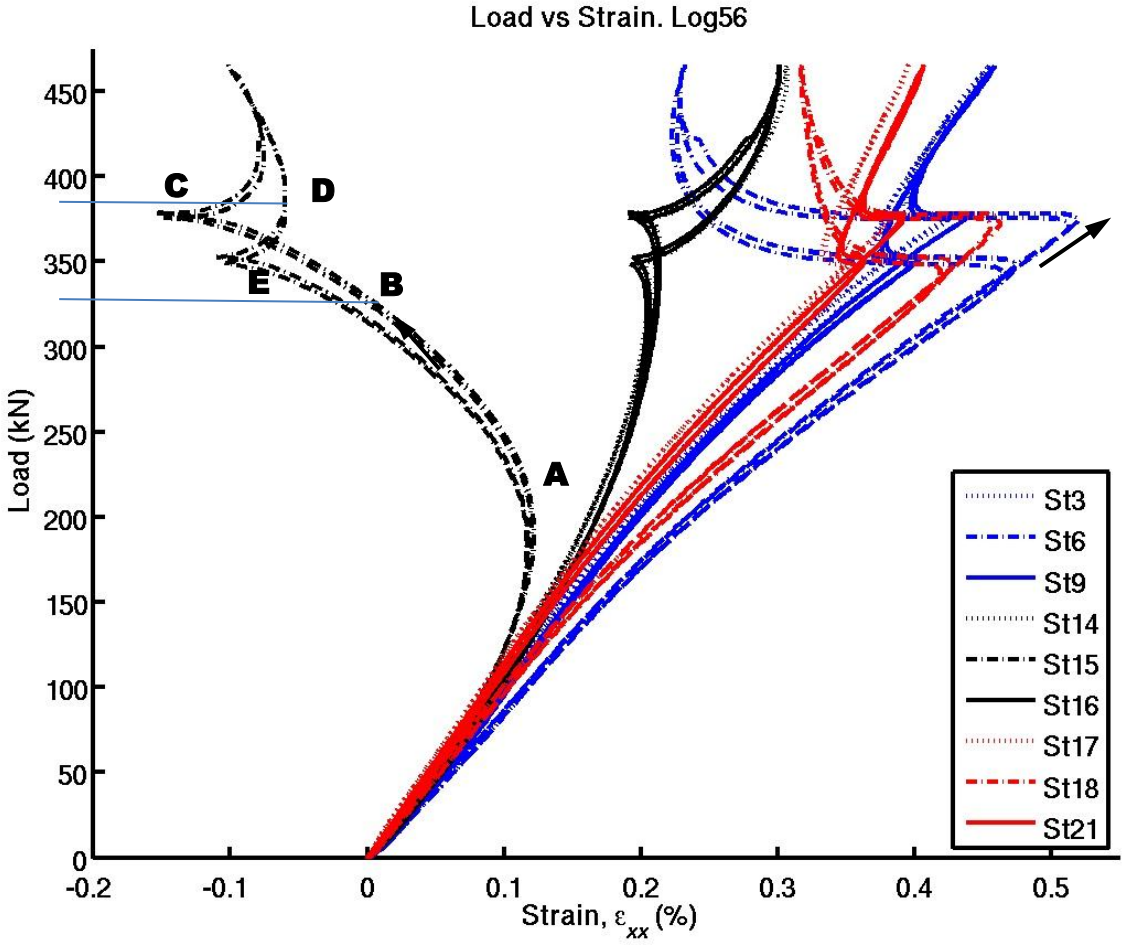

Figure 3.19 Strain for gauges on the smooth side of the skin. Log 56

Visual inspection of the stringer-side of the panel at 509 kN in Log 58 explain why gauge 6 and 18 don't follow each other above 280 kN in Fig. 3.20. It is observed that the stiffener flanges on the lower half of the panel are bending towards each other, and it is even more clearly seen how the stiffeners bend on the upper half, such that the distance increases between their free edges. The free edge of the stringer at Y=100 (left on stringer side) is 'S'-shaped, while the other stringer is a mirror image. The curves shown in Fig. 3.20 give no indication of damage when unloading from 509 kN. The highest residual strain (not shown) after unloading in Log 58 cycle 2 was only 21. μStrain and 24. μStrain for gauges 35 and 37 respectively.

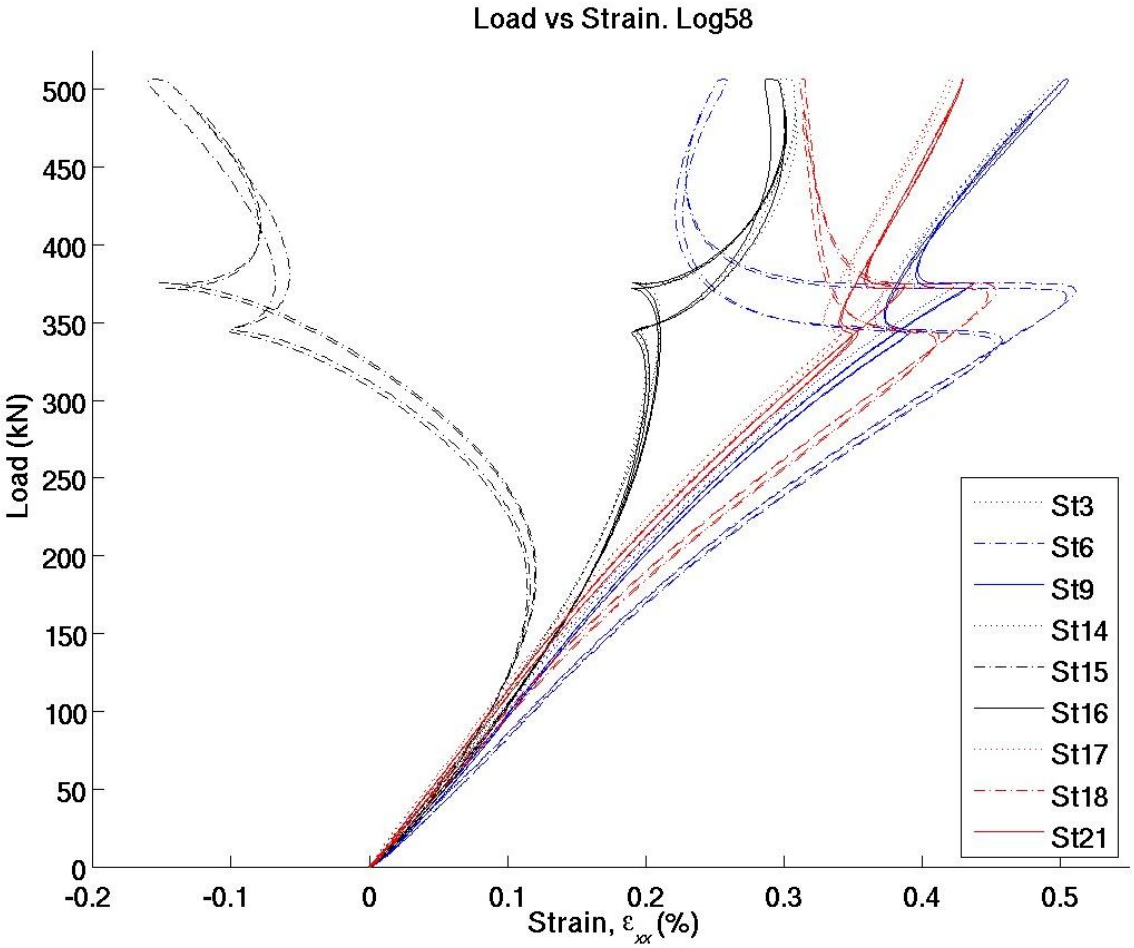

Figure 3.20 Strain for gauges on the smooth side of the skin. Log 58

The initial behaviour during loading in Log 60 is similar to previous cycles, with the mode-switch near 375-380 kN. Then at 522 kN there is a transition in less than 0.5 seconds to a different shape. As seen in Fig. 3.21 the strain curve during unloading for gauge 15 in the middle of the plate is completely different from the path taken during loading. The two curves in Log 62 follow the unloading path in Log 60 until the testing is terminated. Typical for the curves showing the strain response in Log 60 further below will be the plateau near 375 kN, and a transition at 522 kN followed by a completely different and smooth return path to a value that for some gauges are non-zero at zero load (See sect. 3.4).

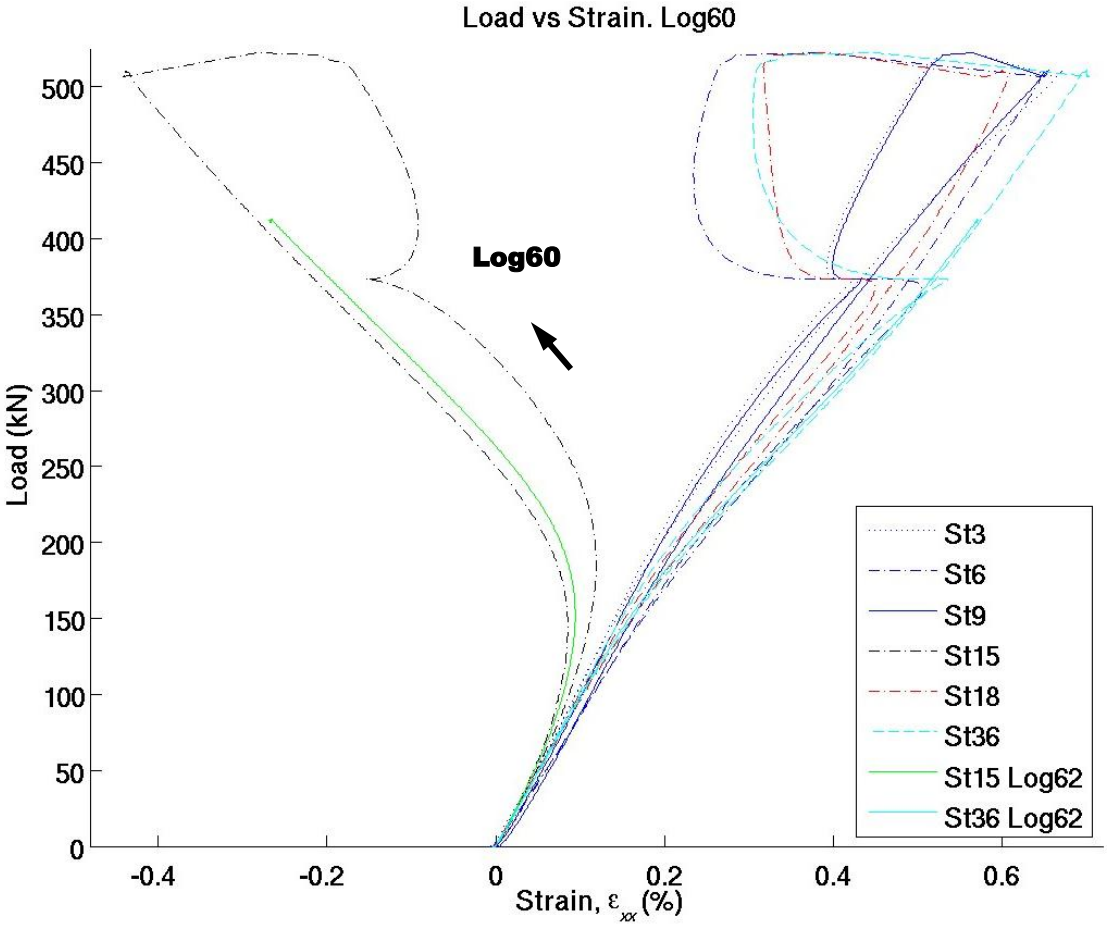

Figure 3.21 Strain in selected gauges during Log 60 and Log 62

The strain in the row at Y=190 will be discussed below. Data for gauge 2 was inaccurate and has been skipped, together with data for gauge 23 on the opposite side of the panel. The strain registration in the loading part of Log 52 cycle 1 is shown in Fig. 3.22. The green curves to the left and the blue curves to the right are for the skin between the stiffeners. Gauge 6 registries 0.46% compressive strain whereas gauge 27 on the opposite side shows a minor tensile strain at 345 kN. Gauges 3, 9, 24 and 30 show the expected good correlation due to the panel symmetry. The agreement between gauges to the far left and right hand side is not as good with a maximum difference of 0.05% between gauges 1 and 34 at 345 kN.

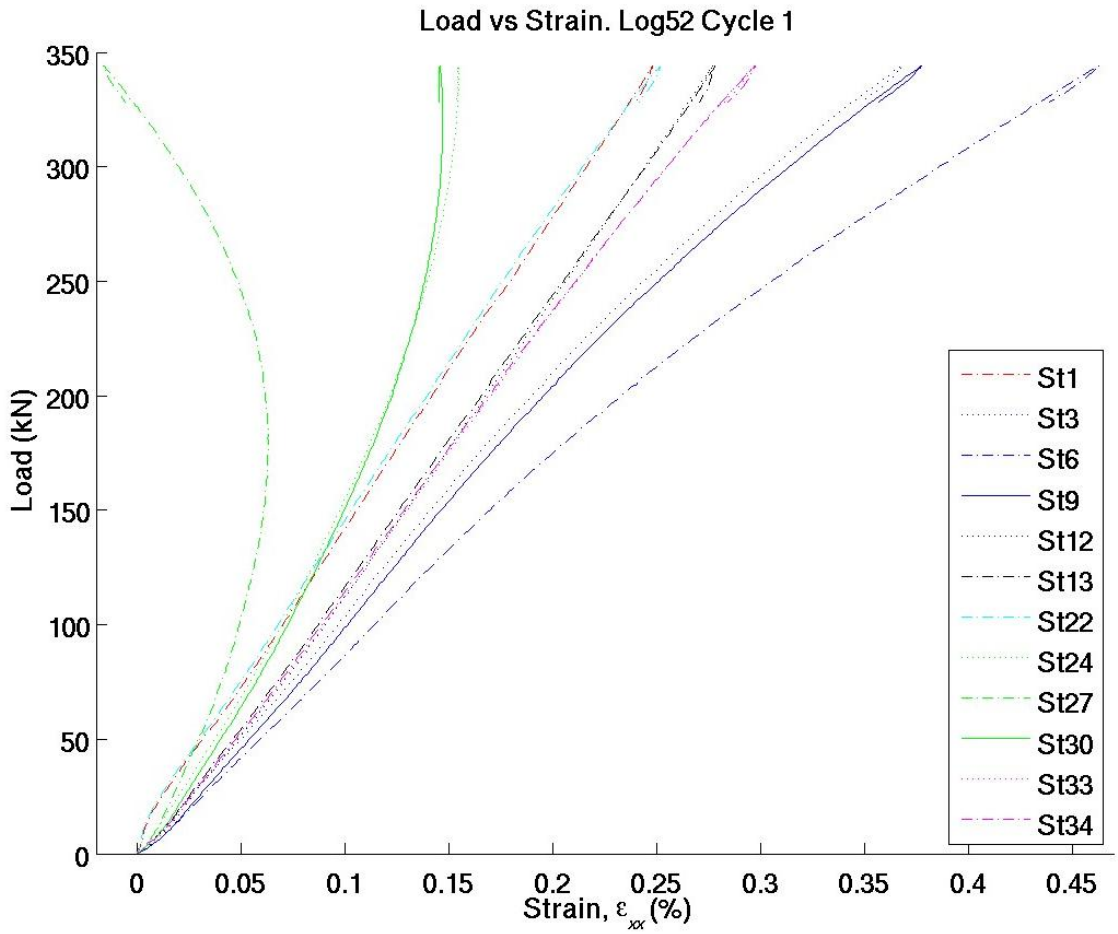

Figure 3.22 Strain in gauges at X=190. Log 52 cycle 1 loading

The average, or membrane strain, for pairs of gauges on opposite sides of the panel is shown in Fig. 3.23. It seems that the stringer at Y=300 carries a slightly higher load than the stringer at Y=100. It is also seen that the middle of the panel does not carry its part of the load, in proportion to the totally applied load. The individual curves for each of the sensors used can be found in Fig. 3.24.

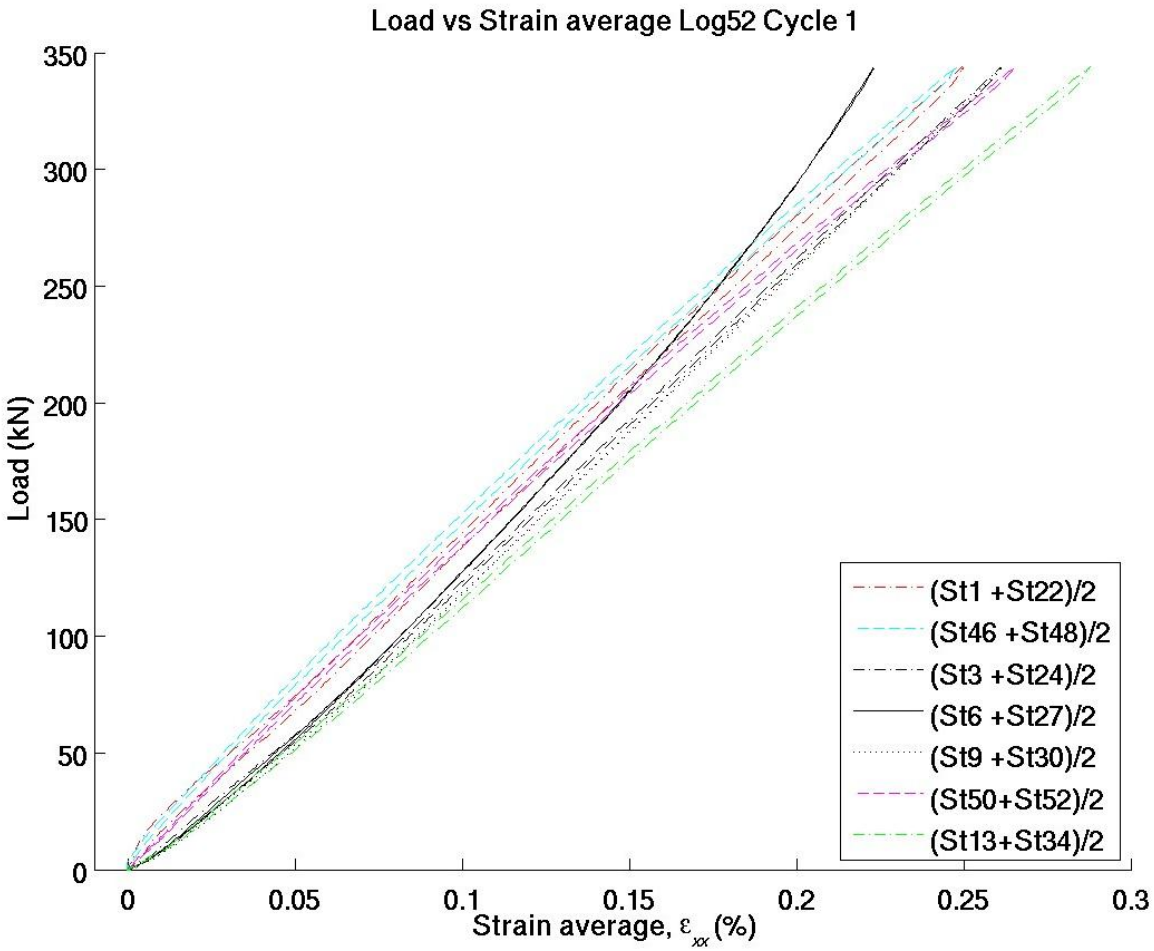

Figure 3.23 Average strain in pair of gauges at X=190. Log 52 cycle 1

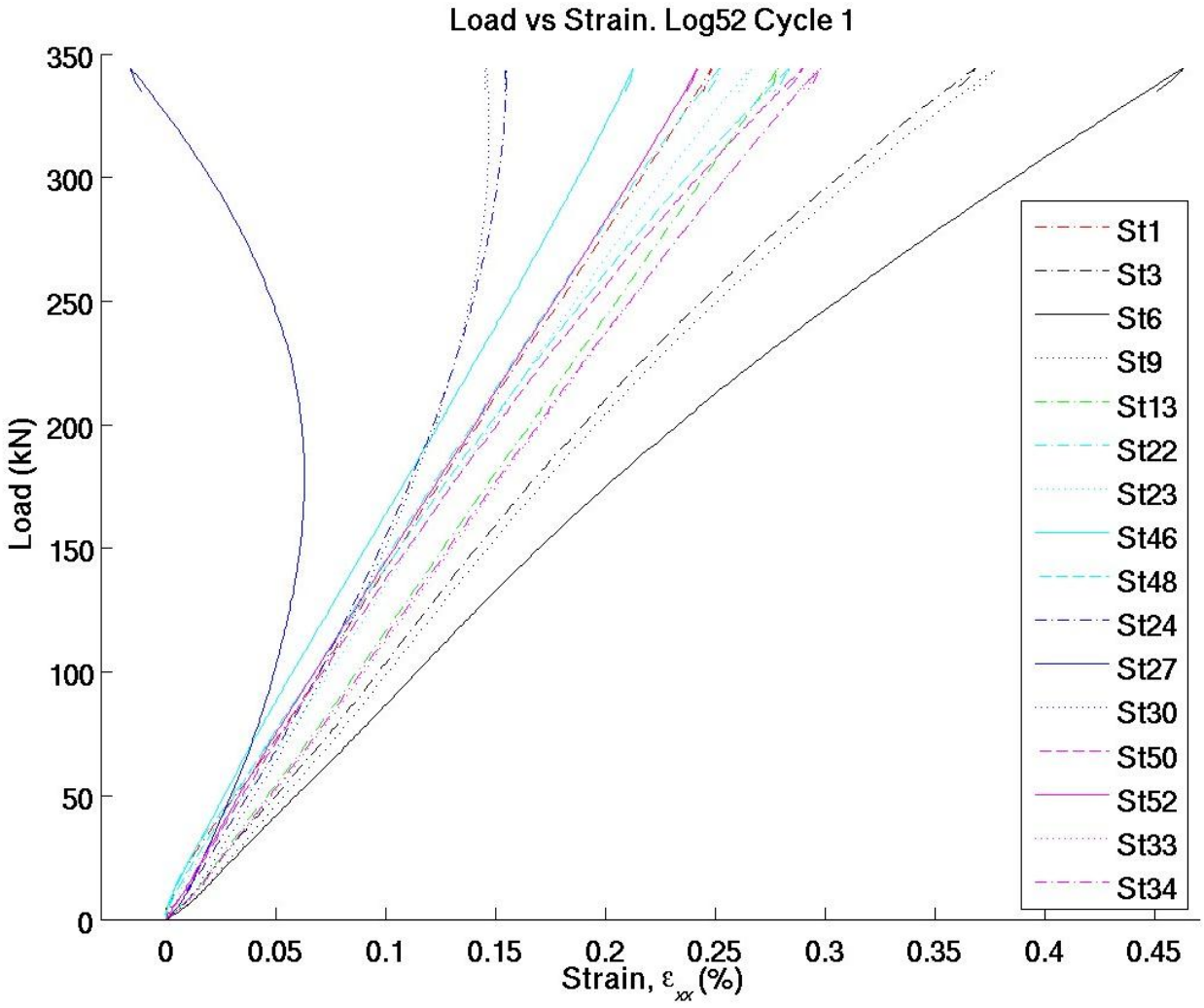

Figure 3.24 Average strain in gauges at X=190. Log 52 cycle 1

The graph for Log 60 corresponding to Log 52 shown in Fig. 3.23 is shown in Fig. 3.25. Something dramatic occurs at maximum load that influences gauges 9&30. The strain is reduced drastically here, while strain increases in the nearby stringer at Y=300 (gauges 50&52).

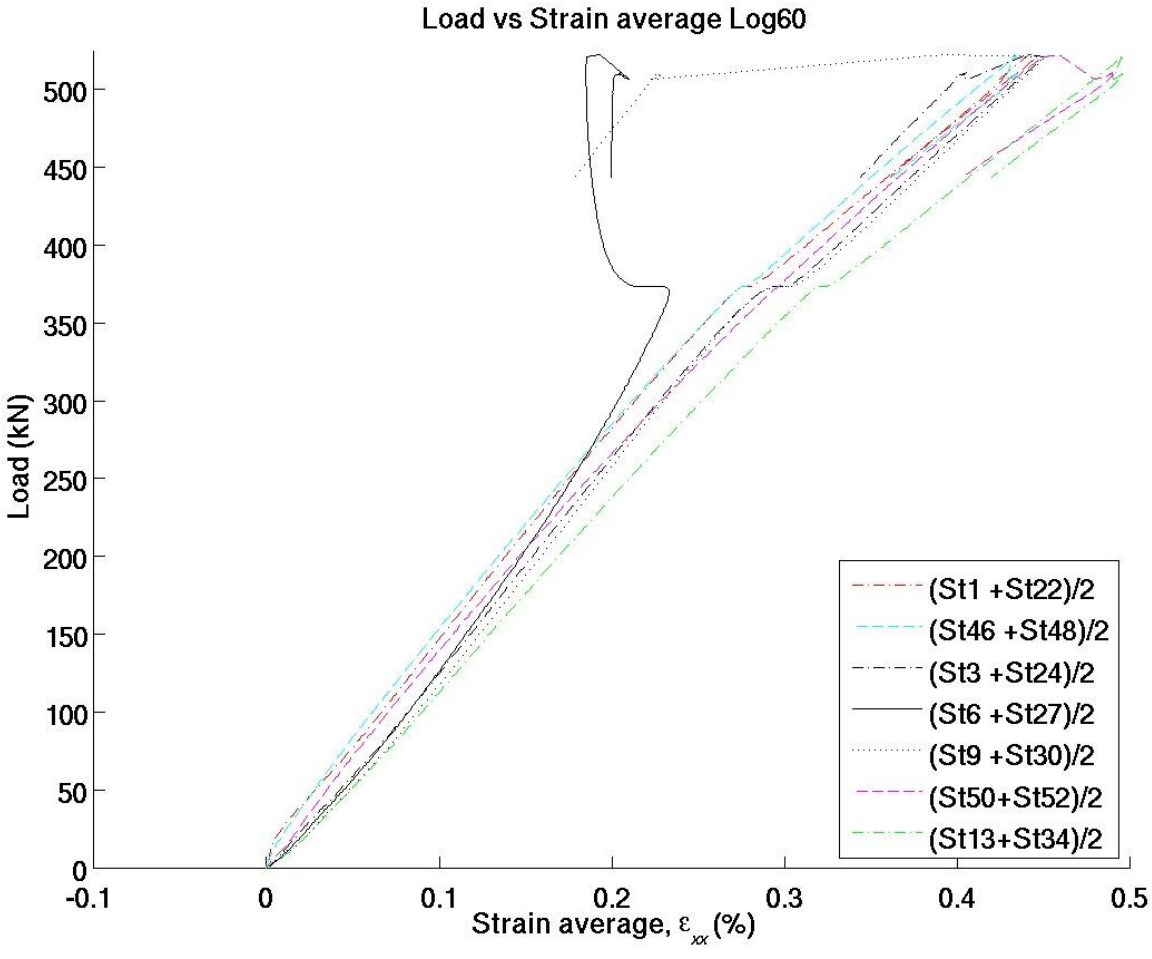

Figure 3.25 Average strain in pair of gauges at X=190. Log 60

The strain difference between points at opposite sides of the skin and stringers are shown in Fig. 3.26. For the stringer at Y=100 it is concluded that some bending is introduced directly as the load is applied. The situation at gauges 24, 27 and 30 is more difficult to evaluate since these gauges are on the lower foot of the horizontal stiffener. It is clear though that the influence by bending increase above about 130 kN.

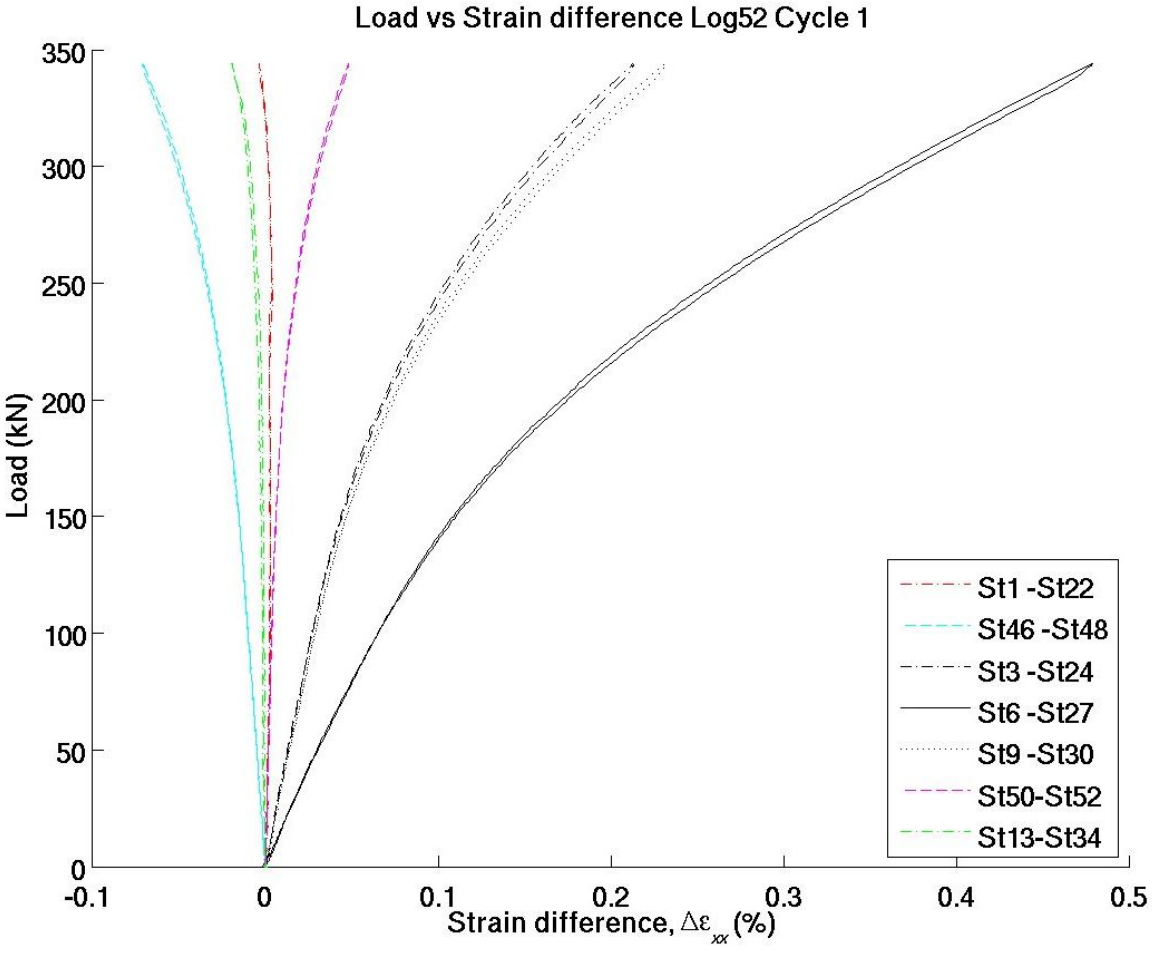

Figure 3.26 Strain difference (bending strain) in pair of gauges at X=190

The curves in Figure 3.27 show the response from gauge 1 in the Logs:50, 54, 58 and 60. As may be seen the response is essentially linear up to 340 kN, with a slope corresponding to a stroke of 0.41 mm/100 kN. The unloading path in Log 60 after reaching 522 kN is initially very nonlinear. The reduction in strain from 0.420% at 522 kN to about 0.33% at 510 kN is fast, taking less than 0.5 seconds. Three red stars have been introduced to mark the actual registrations at 2 Hz.

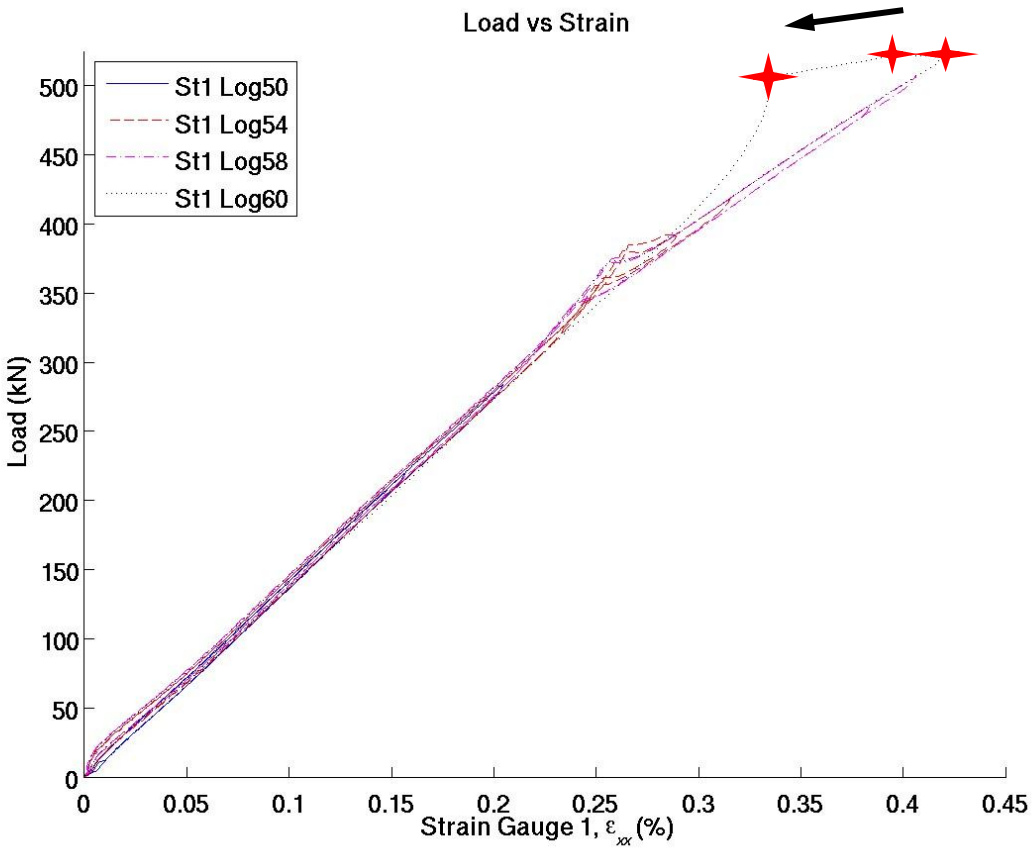

Figure 3.27 Strain responses for gauge one in cycles to different maximum load.

Below are curves for four pairs of rosette gauges with the response in Log 50. When comparing the green curves between Fig. 3.28 and 3.29 it must be remembered that they should be different since the 45-degree direction is anti-symmetric with respect to the vertical plane at Y=200. The other curves show good correlation in general, indicating symmetry in both panel and loading. Strains for gauges 3,6,9 and 18 are scaled with ½ in Figs. 3.28-3.31, as indicated in the legends.

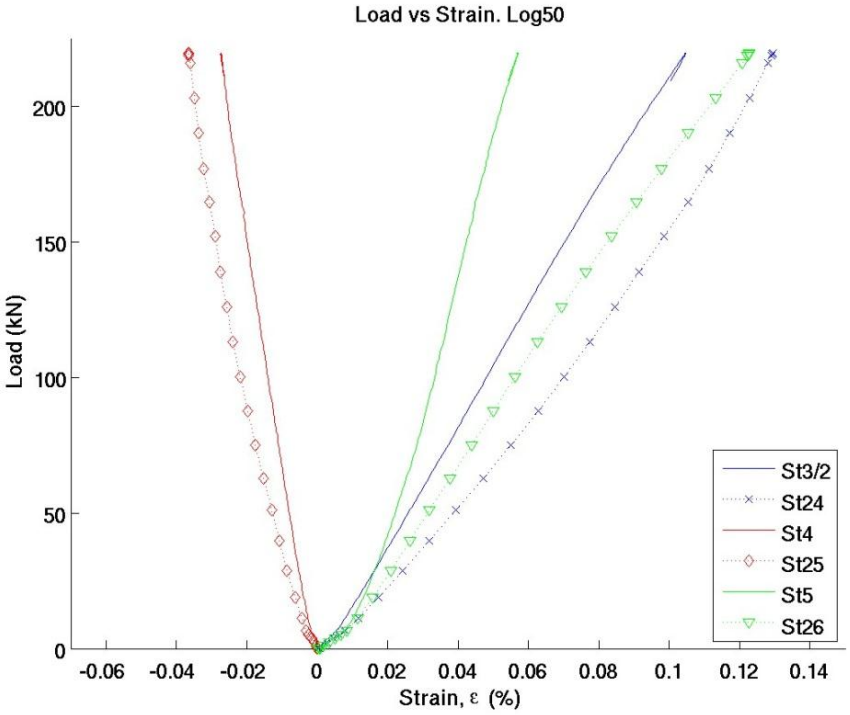

Figure 3.28 Strain in rosettes at X=290 and Y=133

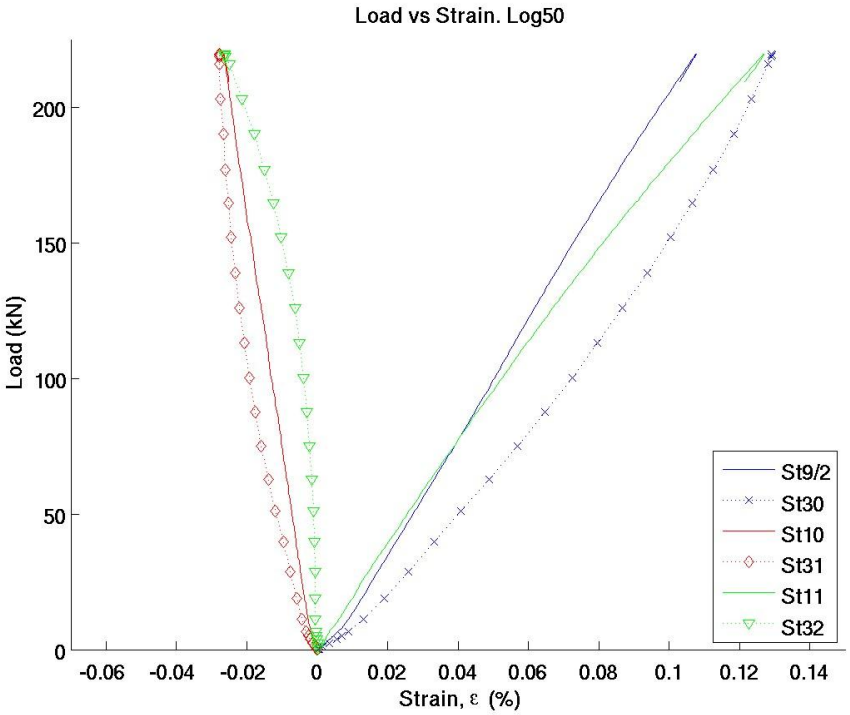

Figure 3.29 Strain in rosettes at X=190 and Y=266

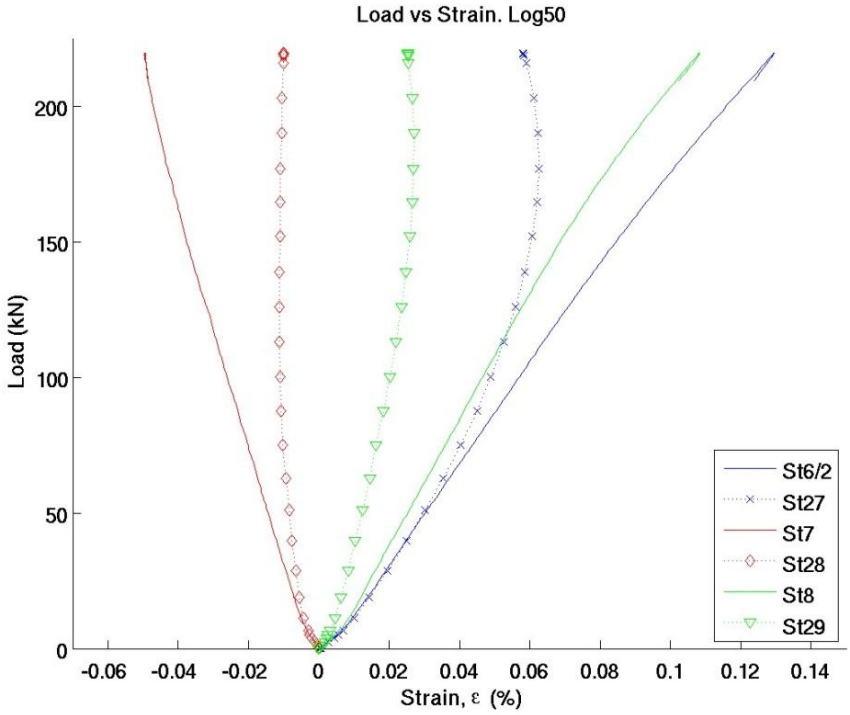

Figure 3.30 Strain in rosettes at X=290 and Y=200

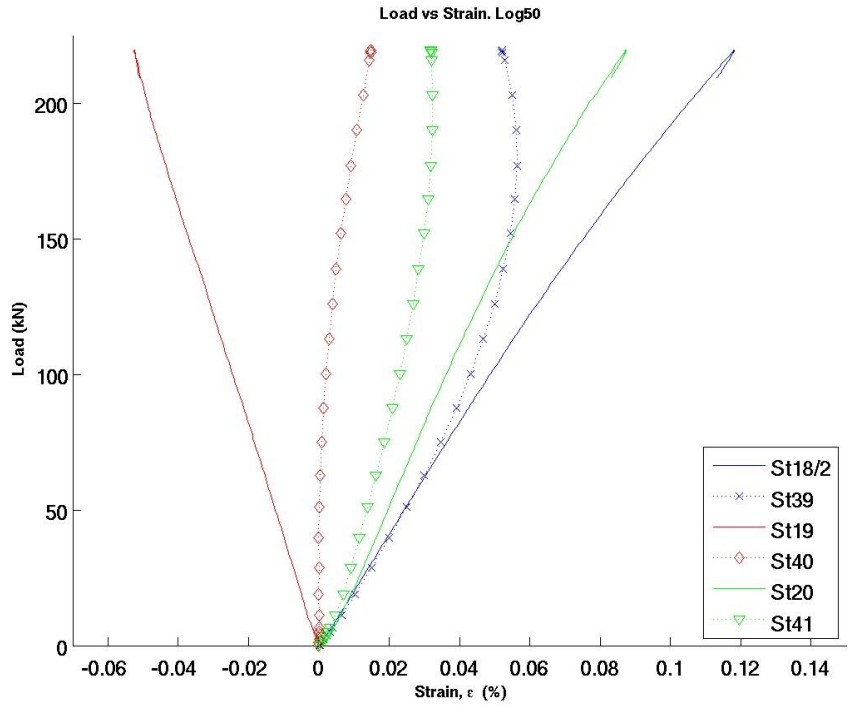

Figure 3.31 Strain in rosettes at X=390 and Y=200

Looking at Fig. 3.32 it is seen that the symmetry in response *wrt.* Y=200 is lost for gauges 24&30, as well as for gauges 25&31 measuring strain in the y-direction, when unloading from maximum load. Significant residual strain after unloading is present for gauges 30 and 31. The plateau near 375 kN during loading is completely missing for all gauges during unloading.

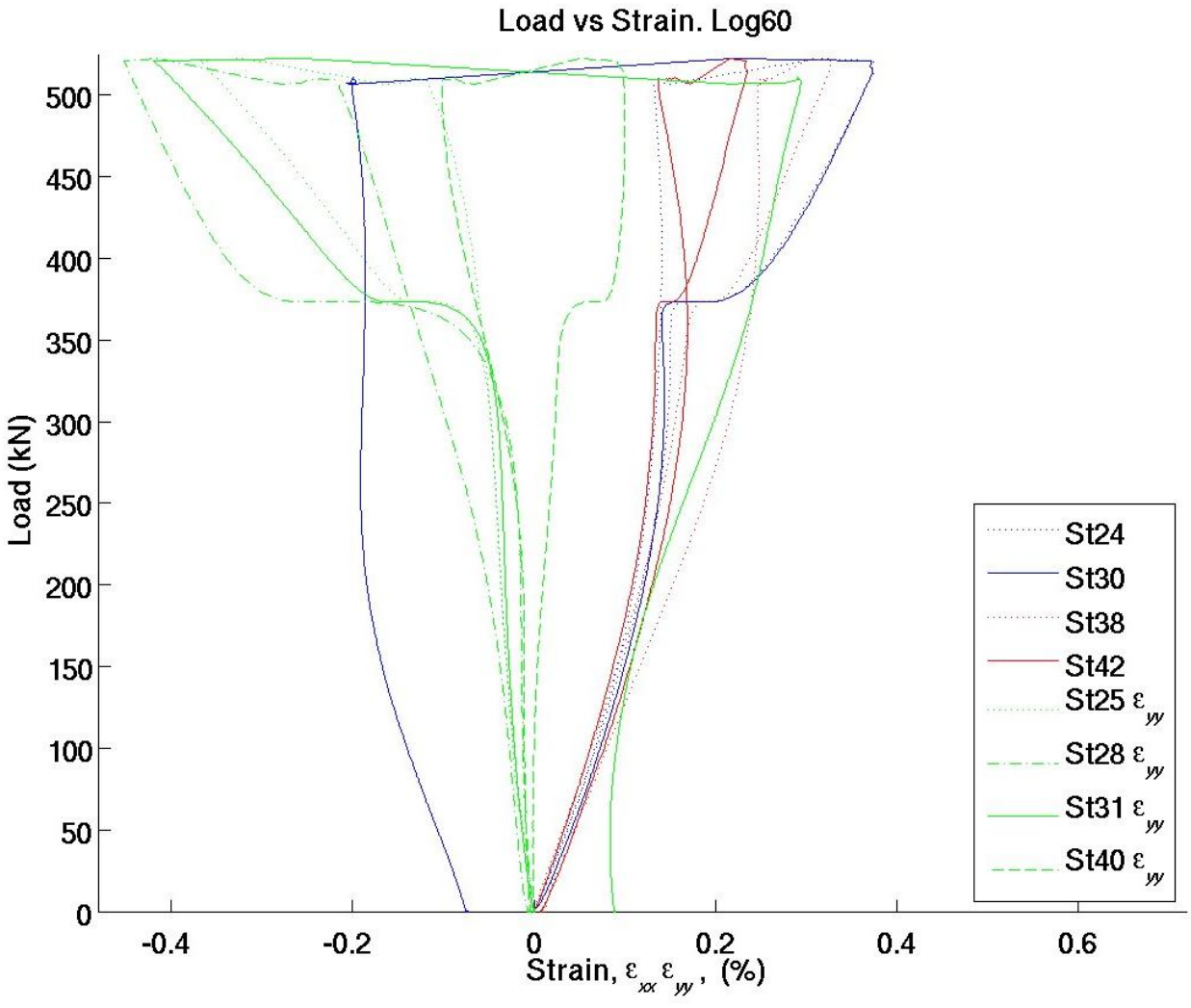

Figure 3.32 Strain in rosettes during Log 60

The tensile z-direction strain in the stringers, near their root, is shown in Fig. 3.33. The strain response in Log 60 is almost identical to the response in cycle one of Log 58 until unloading as may be seen in the same figure.

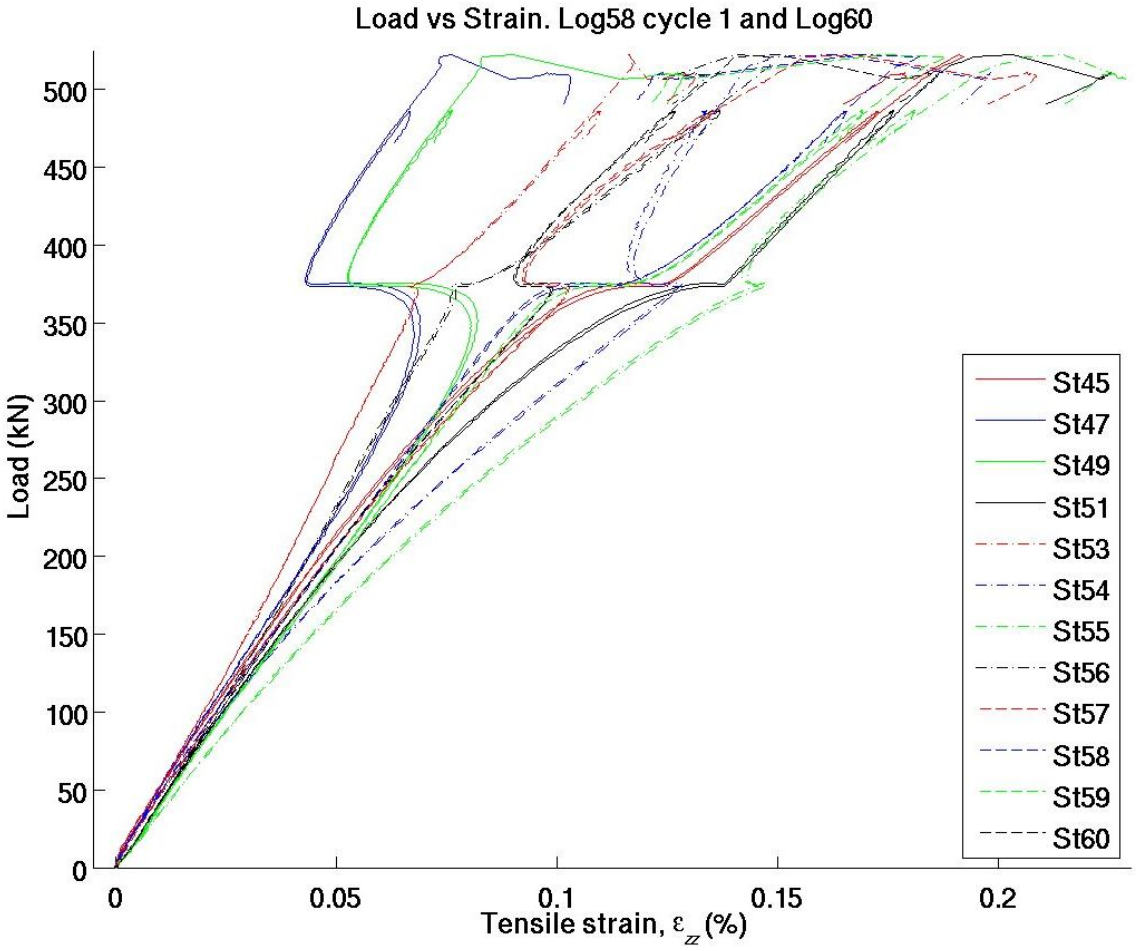

Figure 3.33 Tensile z-direction strain in the stringers, near their root

The average tensile z-direction strain in the left and right vertical stringer is shown in Fig. 3.34. There is a significant strain increase at two locations (Gauges 49/51 and 53/54) when the maximum load is passed.

The average strain in the loading direction for the gauge pair 46,48 shown sign-less in Fig. 3.25 is -0.254% at 350 kN. The corresponding transverse strain determined by using ν_{12} from Table 2.1 becomes, $-\upsilon_{12}\varepsilon_{xx} = 0.3432 * 0.254 = 0.087\%$. As may be expected a line drawn from the origin to (0,087%, 350 kN) in Fig. 3.34 will have approximately the same initial slope as the curves shown for the pair of gauges. This means that the measured strain caused by out-of plane peeling forces between skin and blade is small in general, and negligible below 350 kN.

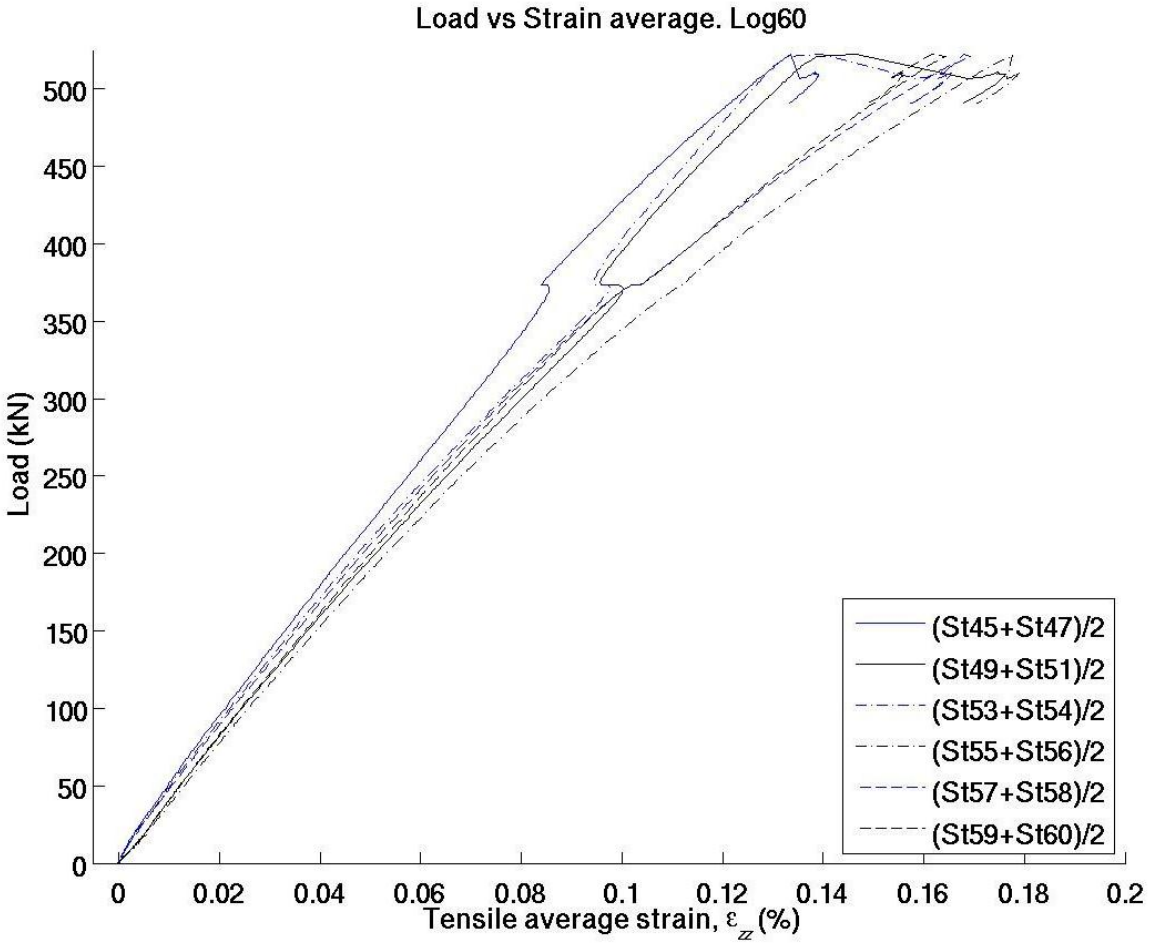

Figure 3.34 Average tensile z-direction strain in stringers

The strain difference (bending strain), in the z-direction in the stringers is shown in Fig. 3.35, for the loading and first part of unloading in Log 60. There is a good symmetry with respect to Y=200 until a load of about 400-450 kN. It is also seen that the stringers in the lower part of the panel (X=390) starts bending in the opposite direction to that for the upper part (X=190) during loading above 375 kN, but the lower part suddenly bends over to the same direction as the upper part when the maximum load is reached.

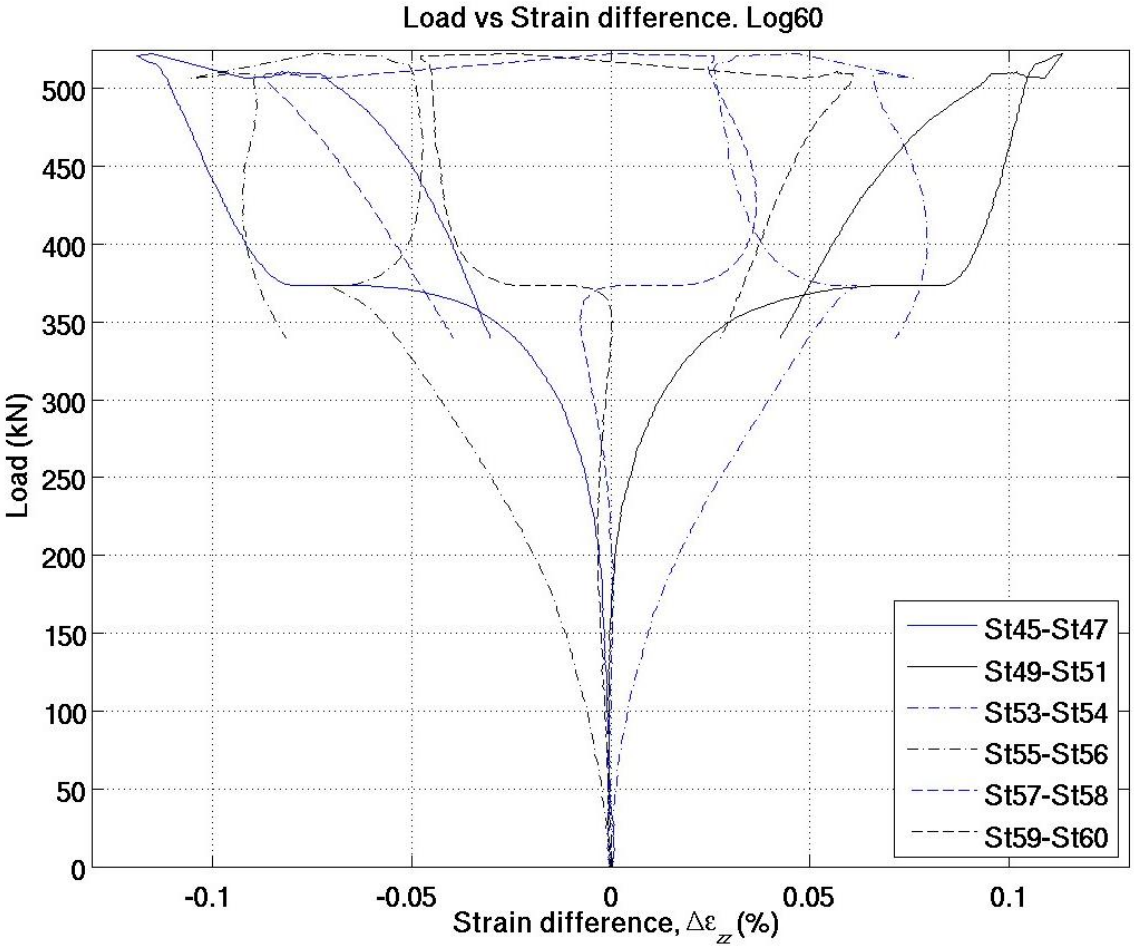

Figure 3.35 Bending strain in stringers near stringer root

For completeness the strain in the two short horizontal stringers (Frame or spar foot) is shown for Log 60 in Fig. 3.36. The levels are very small and correspondence in strain between the upper and lower stringer is completely lost when passing 375 kN during loading.

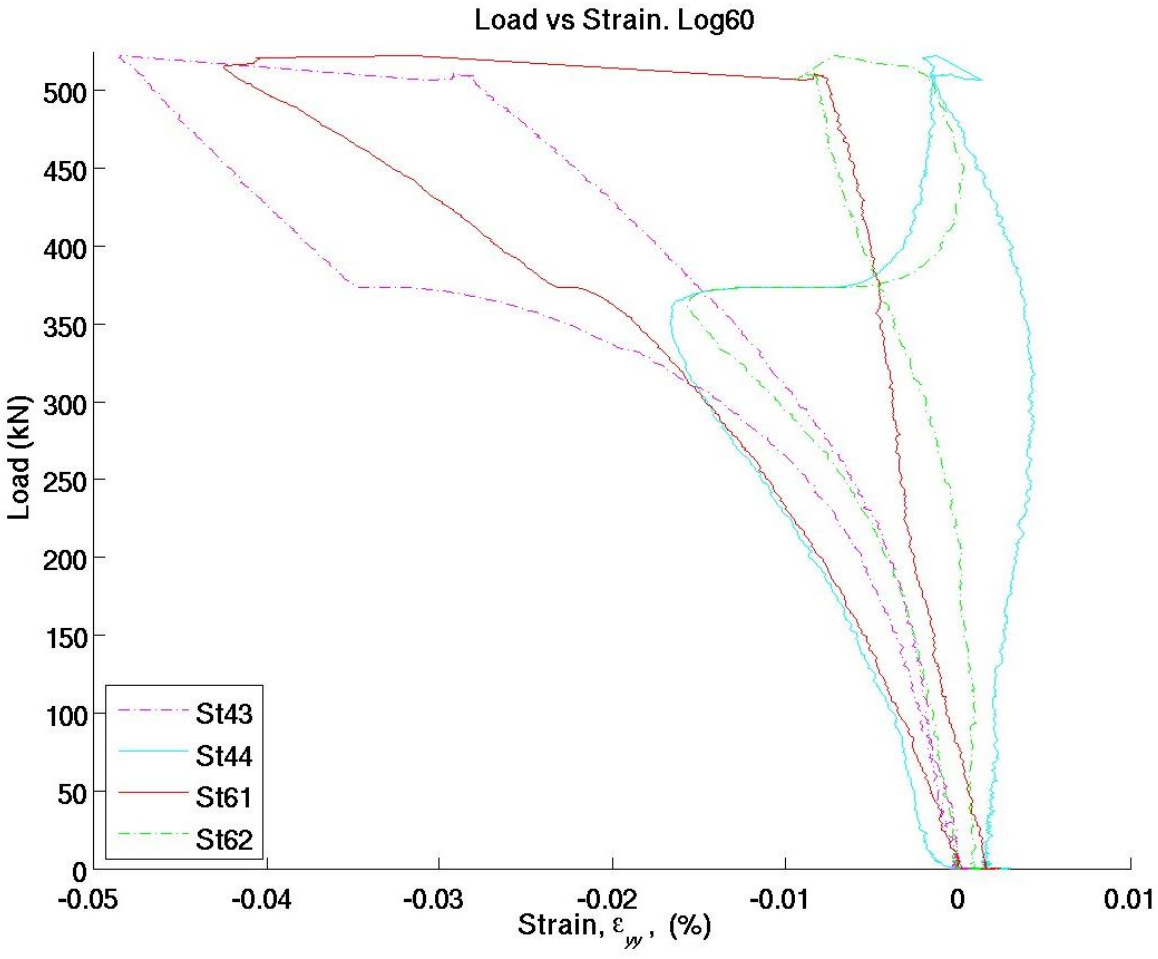

Figure 3.36 Strain in the two short horizontal stringers (Frame or spar foot)

3.4 Residual strain

Barely visible in Fig. 3.21 is the registration of a residual strain of 40 μStrain for gauge 9 after unloading. As may be seen in Fig. 3.21 the load-path in Log 62 resembles the unloading path in Log 60 until the test was terminated at 413 kN, when the load-response was clearly showing a more flexible behaviour than in previous cycles.

Gauge 31 indicates the largest residual strain of all gauges after Log 60 with 884 μStrain. There are eight gauges measuring residual strains higher than 50 μStrain. The values are given in Table 3.1. The values have not been corrected for accumulated residual strain in previous cycles, as the highest residual strain in Log 58 was as low as 23.6 μStrain.

Table 3.1 Residual strain after Log 60

Gauge No.	Residual strain (μStrain)
3	58
6	56
10	63
17	62
30	734
31	884
38	104
42	80

3.5 Post mortem

After failure the specimen was C-scanned and the results are shown in Figs. 3.37 and 3.38. Figure 3.37 is a scan of the central part of the specimen and the vertical "structure" at x'=150 mm is from the vertical stringer. The black vertical area is an echo from the cables to the strain gauges which distorts the signal. The light green areas indicate "delaminations" at approximately 1-1.5 mm depth measured from the smooth side. Since the surface is curved the signal strength varies across the x-direction. A 45^o structure can be seen to the left in both Figures, as if there is a "delamination" at a 45^o ply. To the right in the figures the structure is in the 90^o direction as if there is a "delamination" at a 90^o ply. The two Figures 3.37 and 3.38 are representative for the whole specimen. After failure the specimen was also tested with an A-scan and "delamination"-echoes were detected over the whole surface. This was interpreted as a "delamination" that had propagated over the whole surface out to the edges of the specimen. The C-scans made after the specimen had been removed from the rig can be interpreted as manufacturing consequences resulting in delaminations, or a large delamination which is closed at many places, making ultra-sound passing through it. It is not possible to see any delaminations at the edges with naked eye. Unfortunately, no C-scan was made before testing begun. During manufacturing an adhesive layer was introduced over the complete specimen at the depth where "delaminations" were observed. It is likely that the "delaminations" are actually reflections from this adhesive layer and that these echoes are not due to any failure of the specimen. There is a possibility that the observed drop in force is due to some movement

or fracture in the attachment of the specimen to the rig, and that the specimen is not yet broken.

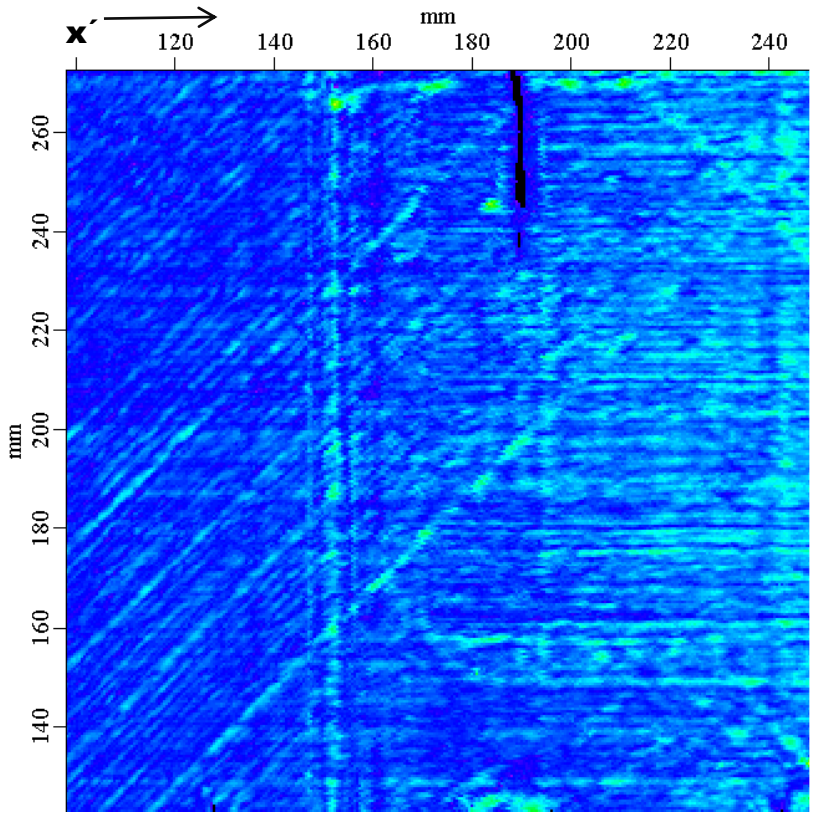

Figure 3.37 C-scan from central part of specimen

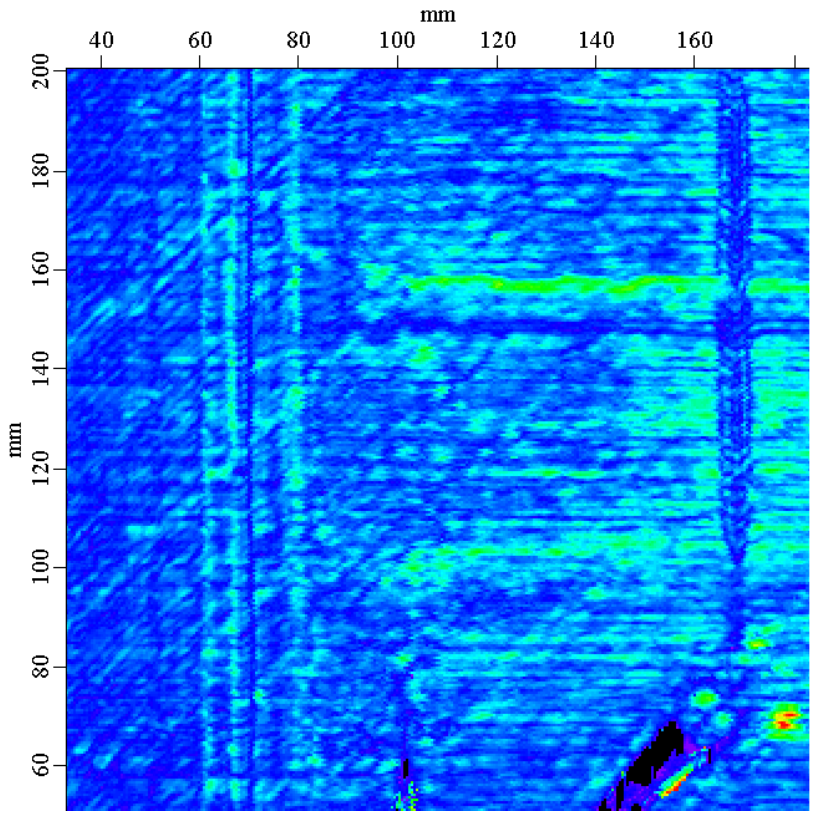

Figure 3.38 C-scan from lower part of specimen

4 Summary and Conclusions

An integral composite structure has been tested in compression to failure to study the effect of buckling. The buckling displacement shape was registered with optical technique and evaluated with the ARAMIS-system. A total of 62 strain gauges were used to record detail strains in the specimen. C-scan and A-scan were used for post-mortem examination, as there was no visible damage to the specimen after the final load-cycle, although significant residual strains were measured. The scans were however not conclusive, as the dominating echoes are likely to be caused by an adhesive layer introduced during manufacturing of the panel.

Strain reversal was observed at 195 kN and the panel has been loaded to successively higher loads nine (9) times before the first indication of possible damage occurred at a load being about 2.5 times higher. A drastic mode-switch occurred at 375-380 kN and the panel was loaded five times to higher loads before damage was indicated. The collapse at 522 kN was spectacular and very sudden, but the panel showed a surprisingly high residual strength. The panel was finally loaded to 413 kN before a clear reduction in axial stiffness was observed, and the test was terminated.

It should perhaps be remarked that in the test condition there is a central part of the panel that is prone to buckling and a surrounding region with the stiffeners which is fairly well supported by the test-rig. This design can as shown give very high collapse loads. Conditions where the stiffeners are less supported can be expected to show a lower ratio between collapse load and buckling load.

The test has shown that the load-carrying capacity of the panel is significantly higher than the buckling load. It has also been shown that a few load-cycles with maximum amplitudes much higher than the buckling load can be applied without causing damage to the panel.

FOI, Swedish Defence Research Agency, is a mainly assignment-funded agency under the Ministry of Defence. The core activities are research, method and technology development, as well as studies conducted in the interests of Swedish defence and the safety and security of society. The organisation employs approximately 1000 personnel of whom about 800 are scientists. This makes FOI Sweden's largest research institute. FOI gives its customers access to leading-edge expertise in a large number of fields such as security policy studies, defence and security related analyses, the assessment of various types of threat, systems for control and management of crises, protection against and management of hazardous substances, IT security and the potential offered by new sensors.

FOI
Defence Research Agency
SE-164 90 Stockholm

Phone: +46 8 555 030 00
Fax: +46 8 555 031 00

www.foi.se